Fall 2017

Block Copolymer Nanostructures for Inorganic Oxide Nanopatterning

Krishna Pandey
Missouri State University, Pandey072@live.missouristate.edu

BLOCK COPOLYMER NANOSTRUCTURES FOR INORGANIC OXIDE NANOPATTERNING

A Master's Thesis

Presented to

The Graduate College of

Missouri State University

In Partial Fulfillment

Of the Requirements for the Degree

Master of Science, Materials Science

By

Krishna Pandey

December 2017

BLOCK COPOLYMER NANOSTRUCTURES FOR INORGANIC OXIDE NANOPATTERNING

Physics, Astronomy and Materials Science

Missouri State University, December 2017

Masters of Science

Krishna Pandey

ABSTRACT

Self-assembled nature of block copolymer (BCP) makes them ideal for emerging technologies in nanometer scale. The micro phase separation between two or more dissimilar polymer blocks of BCP leads to uniform periodic nanostructures of different domains of dimension in the range of 5-100 nm, good for the development of emerging microelectronic and optoelectronics devices. Molecular weight and chain architecture of each blocks govern the morphology evolution; gives different structure like spherical, micelles, lamellae, cylindrical, gyroid etc. The morphology evolution of BCP nanostructure also depends on different external factors as well. In the first work of this thesis, three external factors temperature, BCP thickness and brush layer which influences microphase separation and orientation of the BCP have been varied to study their influence on a cylinder forming BCP poly (styrene-block-methyl methacrylate (PS-b-PMMA). The well-organized periodic nanostructure of BCPs can be used as template to make inorganic nanopattern. In this work, titanium dioxide (TiO_2) with unique structural and functional properties has been selected as inorganic material. In the second and third work of this thesis, I have used the same cylinder forming PS-b-PMMA as a template to deposit TiO_2 nanodots using two different inorganic deposition methods. In the second work, room temperature pulse laser deposition (PLD) and in the third work wet chemical method were used to deposit TiO_2 nanodots. Scanning electron microscope (SEM), energy dispersive x-ray spectroscopy (EDS), x-ray diffraction (XRD), and photoluminescence (PL) were used to characterize BCP and TiO_2 nanostructures.

KEYWORDS: microdomain, nanofabrication, self-assembly, microphase, lithography

This abstract is approved as to form and content

_____

Mahua Biswas, PhD
Chairperson, Advisory Committee
Missouri State University

BLOCK COPOLYMER NANOSTRUCTURES FOR INORGANIC OXIDE NANOPATTERNING

By

Krishna Pandey

A Master's Thesis
Submitted to the Graduate College
Of Missouri State University
In Partial Fulfillment of the Requirements
For the Degree of Masters of Science, Materials Science

December 2017

Approved:

_____
Mahua Biswas, PhD

_____
Robert A. Mayanovic, PhD

_____
Ridwan Sakidja, PhD

_____
Julie Masterson, PhD: Dean, Graduate College

ACKNOWLEDGEMENTS

I am thankful to my research advisor, Dr. Mahua Biswas for her continuous support and guidance at all time during my two years research work. Her door was always open to me for any questions. I highly appreciate for the encouragement, motivation she has provided me in my research and academic activity. Her continue support for attending conferences, appreciation on new ideas, and demand for a high-quality research work have prepared me to take upon the new challenges of the future.

I would like to thank my research committee members Dr. Robert A. Mayanovic, Dr. Ridwan Sakidja for their interest in my work. I am also thankful with Dr. Kartik Ghosh for the useful comments, remarks, and engagement in my academic and research performance.

I am grateful to Rishi Patel for his continuous support on characterization of my samples. I want to thank Calbi Gunder, Samiul Hasan, Shafiqul Islam, Ning Bian, Ahmed Rayhan Mahbub and all graduate students for their direct and indirect help.

I am thankful to my parents, wife, and daughter for their inspiring presence in my life.

TABLE OF CONTENTS

LIST OF FIGURES

INTRODUCTION

Background

Fabrication of nanoscale structures and studying their science "Nanoscience" is the key point for the innovation of new emerging technologies in different fields [1]. The reduction in size of the materials into nanoscale leads to quantization of electronic states, new and striking electrical, thermal ,magnetic ,optical and mechanical properties [2]. The use of nanomaterials for the fabrication of different optical, magnetic, chemical, biomedical and microelectronics devices has received tremendous attention because of lower power consumption, faster response and higher performances [1]. Top-down and bottom-up are two basic approaches which are carried out to fabricate such a nanostructure. In top-down method, precise and small structures are fabricated from macroscopic objects through various ways whereas in bottom-up process, structure are fabricated through the assembly of atoms, molecules or other even smaller objects [3]. Photolithography, laser scanning, serial writing with charged particles, micro and nanomachining, direct writing and ball milling are widely used top down method, whereas various vapor deposition methods (such as chemical vapor deposition, atomic layer deposition, pulsed laser deposition), patterning through self-assembly of block copolymer, colloidal synthesis etc. are the common bottom-up approach used to fabricate nanomaterials [4-8].

Photolithography-a well-developed and successful technique for nanofabrication is limited to industrial implementation because of high cost in photo resist materials, masks and equipment; moreover, this process is facing its limitation to be extended

beyond the 22 nm node with nanolithography [9]. Nanostructures grown using other bottom up methods like chemical vapor deposition and colloidal synthesis usually are non-expensive in nature and mostly show good structural, electrical and optical properties, in practice these methods are not yet self-sufficient enough to produce multiple aspect-ratio (3D hierarchical), reproducible, well-ordered and large area patterns for devices. In this perspective, self-assembled materials for direct synthesis of nanostructures or as templates have received significant attention in the industry for well-ordered and wide area patterning. Specifically, use of self-assembled behavior of block copolymer (BCP) for patterning the materials into nanoscale size 5-100nm with different shape is receiving significant attention recently [1,10–12]. By tuning molecular composition, chain architecture and chemistry of the BCPs, different varieties of nanopattern can be fabricated [13,14]. In my thesis work, a facile, low cost and effective nanopatterning method using BCPs was adopted and self-assembly of BCP molecules to form nanostructures and nanofabrication procedure using BCPs will be discussed in detail.

Block co-polymer and self-assembly property

Block copolymer molecule. In chemistry, a Monomer is defined as, a molecule of any of a class of compounds, mostly organic, that can react with other molecules to form very large molecules, or polymers. A molecule consisting of many repeated Monomer is called Polymer. If two or more homo polymer blocks connected at their ends via covalent bonds is called block co-polymers. The number and types of polymer and the way they link with each other determine the molecular structure of block copolymer.

If a homo polymer chain of monomer A is connected covalently with the homo polymer chain of monomer B, as shown in figure 1, called di-block copolymer. Similarly, the covalent bond between three physically and chemically different block copolymers, A, B and C gives triblock copolymer.

If these blocks arranged randomly give random copolymer, the average size of block copolymer is usually defined in terms of number average molecular weight (M_n) and weight average molecular weight (Mw), is given as;

$$Mn = \frac{\sum_i (n_i M_i)}{\sum_i n_i} \quad ; \qquad Mw = \frac{\sum_i (n_i Mi) \times M_i}{\sum_i (n_i M_i)}$$

Where ni is the number of molecules with molecular weight Mi. The polydispersity index is the ratio of Mw/Mn and is equal to 1 for a monodisperse system.

Block copolymers usually have quite low polydispersity indices (Mw/Mn < 1.1[15,16].

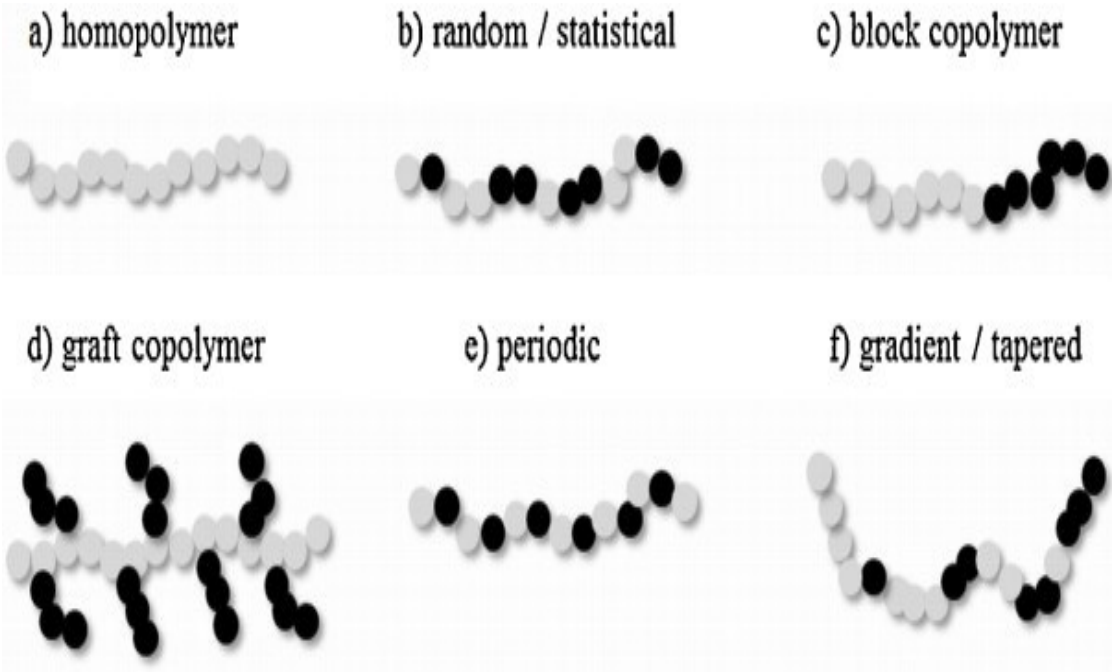

Figure 1. Schematic representation of different types of copolymers consists of multiple homopolymers.

The effective volume of block copolymer is given as,

$$V=\frac{M_A}{\rho_A}+\frac{M_B}{\rho_B}+\ldots.$$

Where M_A and M_B are number average molecular weight of block A and B with corresponding density ρ_A and ρ_B. The effective volume fraction of blocks can be expressed in terms of number average molecular weight (M_A or M_B)

$$f_X=\frac{V_X}{V}=\frac{M_X}{\rho_X V}$$

Where VA is the volume of a homo polymer corresponding to the monomer A. The average number of segments per copolymer (N) is,

$$N=\frac{V}{Vref}$$

And average number of segments in a block A is

$$N_X=\frac{V_X}{Vref}=f_X N$$

The covalent bond between the individual blocks of polymer prevent the macroscopic phase separation even when the polymer blocks are thermodynamically incompatible [15,16]. Despite that, the individual blocks can go for microscopic phase separation into nanoscale domain size below the range of 5-100nm with the influence of external influence like heat. The microphase separation of individual block known as self-assembly property (will be discussed in detail in next section), leads to regular and uniform arrangement of nanodomains which have different chemical and physical properties. The uniform regular arrangement of nanodomains can be used in different nanotechnology fields for device realization.

Intermolecular force involved in self-assembly. The spontaneous process which promotes nanoscale materials pack into regular arrangements by attaining minimum free

energy through minimizing repulsive force and maximizing the attractive molecular interaction is called self-assembly. In other words, self-assembly is a spontaneous chemical process where entities within a mixture arrange themselves in a structured manner and these processes take place in normal chemistry environments [16]. In this process, it is assumed that the system with defects has higher energy states, so, any changes will lead to decrease in energy of the system. As it is go low, a driving force acting on it, which provides the regularity in those nanoscale entities [17].

The self-assembly does involve many kinds of intermolecular forces. Which are classic polar forces including ionic, ion-dipole, dipole-dipole and hydrogen-bonding and hydrophobic interactions. The Π-π interactions and weak covalent forces such as coordination forces have been associated with self-assembly. Π-π interactions have importance in block copolymer self-assembly because of the potential for stacking. These latter forces may have relevance because they can accommodate classic inorganic chemistry to be applied to design systems [19].

Microphase separation. The phase separation only occurs in microscopic scale not in macroscopic. It takes long time because of the mass transport limits on large number of polymer units. The polymer subunits do not have sufficient energy to mobile themselves, so these units need external energy to get mobile and arrange in regular and uniform fashion [14]. i.e. the phase separation only happens when polymer is annealed around the glass transition temperature. The molecular weight also plays a role in chain mobility and interaction strength of the whole system, leading to microphase separation. In BCPs, complete phase separation of chemically distinct sub-groups cannot be achieved because of the chemical covalent bonds in between two blocks [14]. Thus, the chemical

immiscibility of the monomers which drives polymers to segregate and the restorative entropy cost for the deformation of random structure of the blocks during microphase separation are counter balanced by each other [14]. The balance in repulsive intermolecular forces between blocks and attractive restoring force results the regular periodic structure of microphase separated domains with the structure being formed to minimize the contact area between dissimilar blocks [14].

The thermodynamics involve in the self-assembly of BCP can be express in terms of Gibbs free energy equations,

$$\Delta G_{SA} = \Delta H_{SA} - T\Delta S_{SA}$$

If ΔG_{SA} is negative, the self-assembly process is spontaneous. Where ΔH_{SA} is the change in enthalpy of the process, causes due to the potential and intermolecular forces between the assembled entities. ΔS_{SA} is change in entropy during the process of self-assembly. Generally, entropy of the system would decrease with organization of the system. For the spontaneous self-assembly, the enthalpy term must be negative and more than the entropy term. According to this equation, above a critical temperature the self-assembly do not occur as the second term associated with change in entropy approaches the enthalpy [14].

If the entities are to be relatively large distances apart after self-assembly, the repulsive and attractive forces between the entities need to be relatively high or the potential energy will not provide an effective driving force at room temperature. Also, the increase in space between entities lead to the irregular arrangement of entities; hence, for effective self-assembly there needs to be a balance of the intermolecular forces.

The interaction parameter χ, called Flory Huygens parameter [20] is one of the key parameter which determines the BCP morphology. If a di-block copolymer A-b-B, the χ can be written as,

$$\chi = z\Delta w/kT$$

Where χ is dimensional less, exchange energy per molecule normalized by kT. z is the number of neighbors surrounding one block. Δw is the energy required for a block of A from surrounding A blocks and placing in a B block environment; doing the same for a B block (from a B environment to an A environment).

The change in molar enthalpy during mixing is,

$$\Delta Hm = f_A f_B \chi RT$$

f_A and f_B are volume fractions of block A and block B. If there is no change in volume during microphase separation, the molar change in enthalpy can be written as

$$\chi = Vm\ (\delta_A - \delta_B)2/RT$$

Where δ_A and δ_B are the solvent parameters of A and B blocks respectively. Thus, change in enthalpy during mixing is,

$$\Delta Hm = f_A f_B\ Vm\ (\delta_A - \delta_B)2$$

So, blocks with different solubility parameter will have positive enthalpy of mixing, which leads to microphase separation and self-assembly provided the entropy change associated with this process is not too large to overcome the enthalpy contribution[14].

The entropy change during microphase separation can be written as[14],

$$\Delta Sm/RT = (1/N_A) \ln f_A + (1/N_B) \ln f_B$$

Where NA, NB are the degree of polymerization of each block and is given by,

$$f_A = N_A / (N_A + N_B)$$

Phase diagram. At high temperature, the entropy of a polymer dominates over enthalpy, the polymer melts and distribute even randomly. But below a certain transition temperature, the polymer melts, a microphase separation occurs and form regular periodic nanostructure. Apart from temperature, the structure develop from the microphase separation also depends on chemical difference between blocks A and B, degree of polymerization (N) and relative volume fraction of BCPs (f_A and f_B, where $f_A + f_B = 1$). The phase diagram of the BCP self-assembly can be expressed, in which the product of flory-Huggins parameter (χ) and degree of polymerization) (χ_{AB} N) in Y axes and volume fraction fA in X axes as shown in figure 2 [21].

In phase diagram, the parameter (χAB N) controls the microphase separation of BCP. The region with χ_{AB} N <10, called weak segregation region, generally randomly arranged structure formed due to insufficient thermodynamic driving force to overcome the entropic stretching penalty associated with demixing. When χ_{AB} N>10.5, the microphase separation occurs and specific structure can be formed depending upon volume fraction. Another controlling factor of the microphase separation is volume fraction which lies in the X axes of phase diagram. If $f_A \approx 0.15$, sphere of the minority polymer A will form on the matrix of majority polymer. Increasing f_A to the range of 0.2-0.35 will produce hexagonally packed cylinders of minority polymer on matrix of majority. Further increase in f_A, in the range a gyroid of majority formed with minority at the inner part. At f_A=0.5, a thermodynamically stable lamellar structure will form. But, different polymer would have different interaction parameter χ, would give different structure with varying volume fraction. [14], [22], [23].

Orientation of microdomains. As microphase separation occurred on the BCP, the microdomain can align either parallel or perpendicular to the surface of substrate. Perpendicular alignment of BCP are very attractive for many applications such as making ordered arrays of nanorods and nanodots [24-25,17–19]. To achieve perpendicular orientation, preferential wetting of BCP blocks need to be considered. The phase separation of BCP also depends upon the polymer-substrate and polymer-air interfaces [26]. The blocks which has lower interfacial tension with the substrates preferentially wets it, causes parallel alignment of that block with substrate and other block will follow same direction as the underlying block [26] as shown in figure 3 . If block A is preferred by substrate than B, the block A will be attached first to the substrate and B will follow same direction as A.

For the perpendicular orientation of microdomain, both blocks should have similar affinity towards substrate surface, i.e. the surface energy of the substrate should be neutralized, so that both polymer would have equal opportunity to wet the substrate. The composition, hydrophobicity, surface charges are key factor to control wettability of the substrates [28]. Surface modification using brush layer, application of strong electric field and thermal annealing are common practices to get the perpendicular alignment of microdomain [29–32]. Overall, a combination of factors in different steps of BCP nanostructure fabrication such as the brush layer molecule, thickness of the BCP film and annealing temperature govern the orientation of BCP microdomain.

Block co-polymer nanostructures. Utilization of BCP self-assemble behavior to fabricate nanostructure patterns for various applications has been done different way for example: drop casting, dip coating, and spin coating. In all approach, the polymer is

dissolved into a completely soluble solution. In drop casting method, drops of BCP solution are placed on the substrate and make it to dry. In dip coating method, sample is dipped into the BCP solutions for a while and make it dry. These two methods usually result in a non-uniform irregular thin film and regular and periodic BCP nanostructure cannot be expected from this type of film.

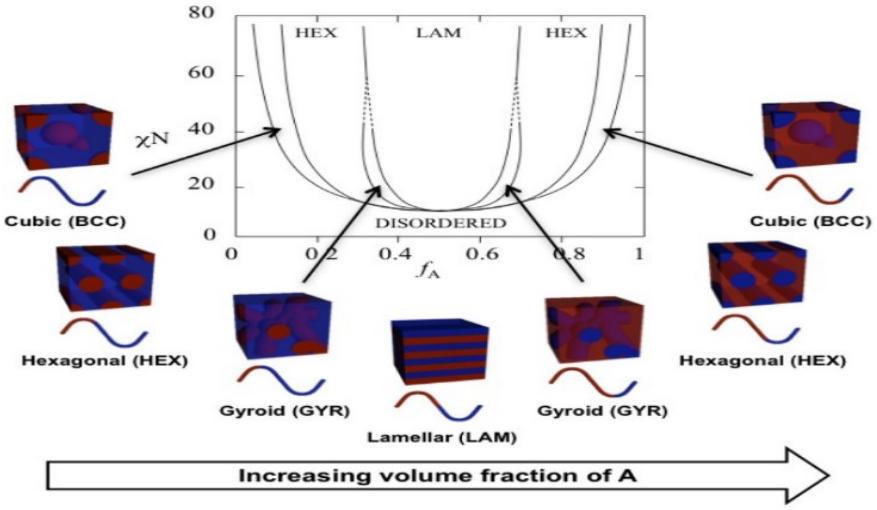

Figure 2. Phase separation of Block copolymer microphase separation[24]

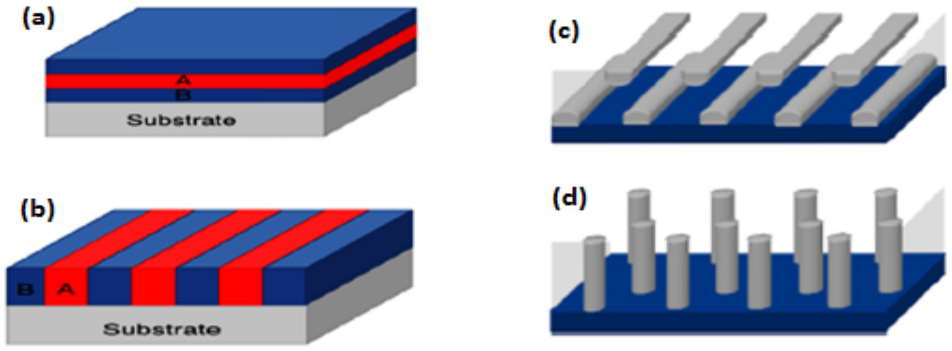

Figure 3. Preferential wetting of the substrate (a) lamellae structure parallel to the substrate (b) Lamellae structure perpendicular to the substrate (c) Cylindrical structure parallel to the substrate (d) Cylindrical structure perpendicular to the substrate [27]

Among three methods, the most promising method is spin coating, in which BCP solution is dispensed on top of substrate and spun with different revolution per unit time (RPM).

The spin coating method results a homogeneous, uniform thin film, from which we expect periodic regular BCP morphology. Along with the solution concentration, molecular weight of BCP, the spin coating parameters and the drying time and condition also influence the characteristic of film. Both static and dynamic dispensed method of spin coating are mostly used. The thickness of the film is governed mainly by the rotation time period of spin coating and solution concentration. The thickness (t) of thin film deposited by using the spin coater is inversely proportional to angular velocity (w) [33] as shown in figure 4.

$$\text{Thickness (t)} = \frac{1}{\sqrt{w}}$$

Role of brush layer, thickness and annealing condition on BCP nanostructures. Brush layer usually a functionalized polymer or random copolymers is used to neutralize the surface energy; allowing perpendicular orientation of microdomains by non-preferential wetting of the substrate [26]. Self-assembled monolayers (SAMs) made from mixture of n-alkane thiols with polar and nonpolar end groups have been used to control the wetting properties of substrate, to get the surfaces with a controlled polar characteristic [11,34-35]. The variation in surface wetting behavior from preferential to neutral to dewetting happen by tuning the grafting density of SAMs [36]. Recently, random copolymers (RCPs) is used extensively as brush layer due to its extra attractive feature than SAMs [37]`. The molecular representation of such brush polymer is shown in figure 5. When polymer chains loss its entropy at the

interface, the brush polymer reduces the entropic driving force for dewetting, which improves adhesion and makes the brush-polymer interaction same all over the surface of substrate [37-38].

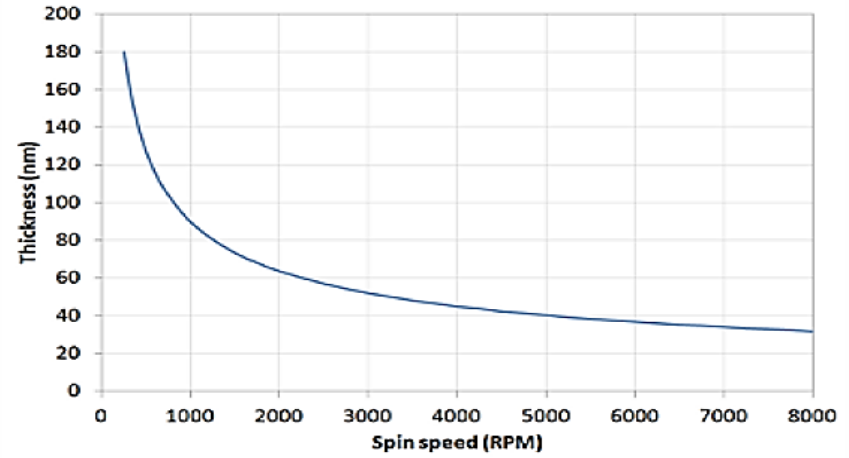

Figure 4. Relation between thickness and angular velocity [33]

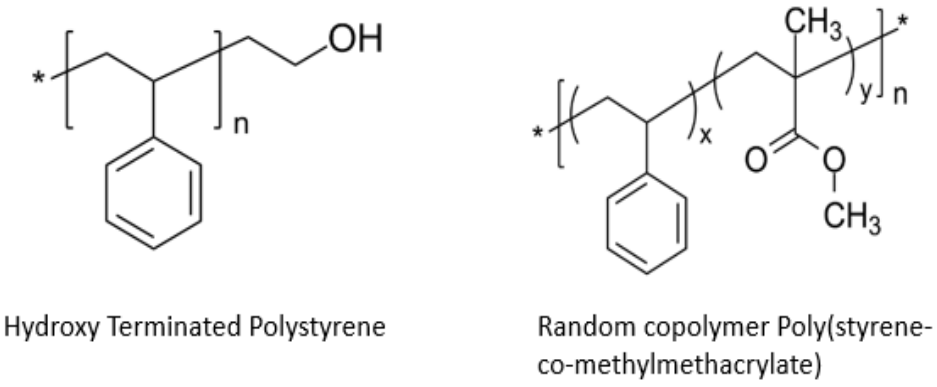

Figure 5. Molecular representation of brush polymer [39,40]

The dissimilarity in interfacial which acts on the blocks of BCP leads to the formation of layering effect on the film [41–44]. In lamellar morphology, one blocks experienced more interfacial force, which align first in parallel to the substrate. For

symmetric wetting condition, same block wets both surfaces, film thickness (t) must be equal to integral of domain spacing. i.e. t= nL0. When two interfaces attract different blocks (asymmetric wetting), the film thickness equals to (n+1/2) L_0. But for spherical and cylindrical forming BCP, the spherical or cylindrical structure will observe when thickness (t) ~ nA+B. where n is integer number, A is sphere-sphere, or Cylinder-Cylinder distance and B is thickness of brush layer [45].

Annealing of BCP above their glass transition temperature will cause microphase separation by minimizing the surface energy and maximizing the interaction with surface, [14]. The segregation force between blocks is the key factor to determine annealing time and temperature at which phase behavior of a BCP can observe. Phase separation is also controlled by a thermodynamic process-order disorder phase transition(ODT), when BCP thin film exhibits a homogeneous morphology with all blocks are completely miscible upon annealing at certain temperature and in reverse, all blocks would be in immiscible due to decrease in temperature-exhibits a heterogeneous state of ordered microphase [46]. Due to weak segregation force, parallel cylinder forming BCP show straightening process before order disorder transition (ODT) and do not show long range composition near ODT. But, perpendicular cylinder forming BCP with strong segregation force shows transition from perpendicular to parallel below ODT [47].

Application of BCP nanostructure. The BCP has huge applications in current technological advancement in the field of biomedicine, biomaterials, microelectronics, photoelectric materials, catalysis etc. [48-49]. One of the attractive application of nanoscale BCP structures are as templates to fabricate thermodynamically stable inorganic and metallic nanopatterns for microelectronics, optoelectronics and biomedical

field [50]. BCP nanostructure can be used as membrane in catalysis, which acts as selective barrier between at least two different compartments and regulates gas, liquid or substance to transport between them [51,52].

The BCP assisted inorganic materials can be used as photonic materials which are designed accordance with periodic domain size, refractive index contrast and morphology [53]. Self-assembled behavior of BCP to arrange into periodic uniform structure are ideal materials to fabricate those photonic materials [54]. Similarly, BCPs are also used as structural directing agent for metal salts or nanoparticles to make bulk hybrid materials [55]. In addition, The BCP micelle structures have promising application in drug delivery inside the human body [56,57]. The patterned nanostructure are also important features used in force sensor to study the cell behavior and cell biology [58,59].

Objective of the thesis. This thesis work can be outlined in three projects as mentioned below-

Study of BCP morphology evolution through microphase separation

(i) BCP templated TiO_2 nanopatterning using solution method

(ii) BCP templated TiO_2 nanopatterning using pulsed laser deposition (PLD) method

Two different polystyrene-block-polymethylmethacrylate (PS-b-PMMA) BCPs were used for this thesis work. In the first project, the BCP nanostructure morphology and orientation were tuned by changing the different variables: brush polymer, thickness of BCP film and annealing time and temperature. In the second and third project, these PS-b-PMMA nanostructures were used as a template to pattern the inorganic oxide materials. In the second project, solution chemistry was used and in the third project room temperature PLD method was used to fabricate ordered TiO_2 nanostructures. Field emission scanning electron microscopy (FESEM), atomic force microscopy (AFM), x-

ray diffraction (XRD), photoluminescence (PL) and energy dispersive x-ray diffraction (EDX) were used to characterize the BCP and TiO_2 nanostructures. The detail background and detail of these projects are described in the following chapters of the thesis.

A STUDY OF BLOCK COPOLYMER NANOSTRUCTURES MORPHOLOGICAL EVOLUTION

Abstract

The ability of self-assembled block copolymer (BCP) to form different morphologies and well-ordered structures is very attractive due to ease of fabrication in nanoscale and compatibility with different systems. These nanostructures provide potential or practical applications in many fields such as biomedicine, biomaterials, micro-electronics, photoelectric materials, catalysis. The BCP film morphology is defined by phase separated microdomain of different homopolymer and depends on many factors during deposition apart from synthesis factors like molecular composition and polymer architecture of BCP. Moreover, orientation of BCP microdomain is determined by strength of interfacial interaction which can be tuned by external interference. In this work, effect of three different BCP nanostructure assembly parameters: brush polymer composition and deposition condition, BCP film thickness, and BCP film annealing time and temperature are systematically studied on one PMMA cylinder forming BCP to show that, the evolution of morphology and orientation is dependent on all these factors and how all these factors are correlated with each other. It is shown that, the uniform periodic nanostructures with perpendicular orientation can be obtained only with proper match of all parameters in a definite window which gives the appropriate surface tension and interfacial energy for perpendicular orientation.

Introduction

Block copolymers (BCPs) have received considerable attention recently due to their inherent self-assemble property which can lead to various nanoscale structures like spheres, cylinders, bi-continuous gyroid, and lamellae, depending on the composition and chain architecture of the BCPs [1]. The well-aligned and periodic nanostructures of BCPs with versatile morphology can be ranged from 5–100nm in size [2]. Therefore these self-assembled polymers are considered for direct and indirect (such as template) applications in biomedicine, biomaterials, microelectronics, photoelectric materials, catalysis etc. [3,4]. Particularly, in nanolithography utilization of self-assembled BCP thin film nanostructure for patterning the substrates, has been widely recognized as an alternative or complementary approach to conventional photolithography [1,5-6].

During phase separation and morphology evolution, a non-equilibrium, poorly ordered and defective nanostructure with mixed morphologies may be formed due to variety of reasons [7]. To get desired structures, achieve long-range order and to control the orientation of the nanodomains, a range of experimental parameters need to be controlled and different post-treatment techniques such as thermal annealing, directed self-assembly on prepatterned substrates, application of mechanical stress and electric field have been proposed [5-6,8]. Understanding and controlling the external deposition factors of BCP nanostructures such as brush layer and annealing temperature is important because applications like microelectronics and biomedical require extremely low defect densities.

Three different external parameters for depositing perpendicular orientation of

BCP cylinders (i) brush layer, (ii) BCP film thickness and (iii) BCP film annealing are varied to show the perfect window for obtaining perpendicular orientation and to understand the morphology evolution due to variation of these parameters. There are numerous report to understand the effect of these parameters individually for different BCPs [9–16] . In this report, a comprehensive study on the influence of these parameters for the orientation of one selecting BCP is presented. The background work on of these parameters on BCP nanostructures evolution are discussed below.

A neutral coating layer/brush layer helps to tune the interfacial energy difference between two blocks at air-substrate interface. Cylinder forming diblock-copolymer typically orient parallel to the film plane, owing to preferential wetting of one of the blocks at the substrate and free interfaces. The wetting behavior of blocks on the surface and the orientation can be controlled by changing substrate air interface with brush layer [9,17]. A brush layer in most of the cases a random copolymer (RCP) with end functional groups like OH and tempo (2,2,6,6-tetramethylpiperidinoxyl) moiety is used before BCP nanostructure self-assembly for the purpose of dewetting, improved adhesion and uniform coverage over a large area by changing the interfacial energy [9]. While studying the effect of brush layer on BCP morphology, Mansky *et al.* have also shown that orientation and ordering of the microphase-separated BCPs can be controlled by controlling the relative interfacial energies between each copolymers block and the substrate [9]. It was shown that, for a same block lengths lamella forming di block copolymers, the lamellae orient parallel to the substrate and plane of the film with substrate-air interface; while by depositing a brush layer and changing the interfacial energies between both blocks and the substrate the lamellae orient perpendicular to the

substrate and plane of the film. Selecting the appropriate molecule as brush layer is vital for the perpendicular orientation and extensive study in this area is necessary for application purpose.

BCP film thickness is one of the factors for parallel and perpendicular orientation of BCP nanostructures [12–14,18-19]. It is widely known that, there is a limited thickness window located in the proximity of lattice spacing or domain size L_0 of the cylinders (center to center distance of cylinders) where perpendicular orientation can be obtained due to commensurability between the thickness of film and lattice spacing [12, 13,20-21]. Only in few works recently it is shown that, perpendicular orientation can be achieved with $L_0/2$ thickness of BCP film as well [14]. With the increase in film thickness from $L_0/2$ to L_0 mixed parallel and perpendicular morphology can be observed, and a complete coverage of parallel orientation was observed at $3/4L_0$ [14]. Further study on BCP morphology and orientation in these thickness windows and beyond will be beneficial for realizing BCP nanostructures in applications.

The annealing temperature is another external experimental parameter which has significance role in defining the orientation of BCP microdomain [22]. Entropy of the system and enthalpy are key factors which governs the thermodynamics of BCP [23]. Although at room temperature the BCP phases are metastable, but no reordering occurs as it is frozen at that temperature. With external energy such as thermal annealing this metastable state tries to reorder through phase separation; usually the phase separation of BCP will not occur until the temperature of system is below glass transition temperature of the blocks. As it reached to the glass temperature, the increase in chain mobility leads microphase separation [24]. The incompatibility between two blocks linked by covalent

bond after annealing treatment organized into different shape and size of periodic structure [25]. The combination proper annealing time and temperature govern the phase separation and orientation of the blocks by playing with the surface tension of each blocks [16,22,26]. There are few independent study on the thermal effect on BCP phase transition and orientation [16,22,26-27]. Further study on the ordering of phases due to thermal effect using different combination of experimental parameters will strengthen the understanding of morphology evolution.

A uniform periodic arrangement of BCP microdomain is result of a perfect combination of BCP thickness, annealing temperature/time along with surface modification via a brush polymer. This study is expected to strengthen the existing understanding of BCP morphology evolution and orientation, specifically on the PS-b-PMMA BCPs. This understanding will help the BCP nanostructure fabrication process more promising and reproducible; which is still a challenge to achieve in different experimental setups.

Experimental details

In this work, all the chemicals were purchased from Sigma Aldrich and all the polymers were purchased from Polymer Source INC.

A1. Substrate cleaning. Silicon (100) with thin layer of native oxide were used for this experiment. A solution of hydrogen peroxide (H_2O_2), ammonium hydroxide (NH_4OH) and distilled water (H_2O), in the ratio of 1:1:5 at 65°C for 2.5 hr. was used to eliminate residual organic traces from the Si surface.

To study the BCP nanostructure morphology evolution, the experiments performed in this study are mentioned below-

1. Effect of different brush polymers
2. Effect of BCP film thickness
3. Effect of BCP film annealing time and temperature

A2. Effect of different brush polymers. In this study, two BCPs Polystyrene-block-Polymethylmethacrylate (PS (M_w 52000)-b-PMMA (M_w 142000)) (named as PS52) and Polystyrene-block-Polymethylmethacrylate (PS (M_w 55000)-b-PMMA (M_w 22000)) (named as PMMA22) were used. As mentioned above, brush polymer is used before BCP deposition to obtain perpendicular orientation of BCP nanostructures. To study the effect of brush layer three different polymers, monohydroxy terminated polystyrene (Mn:9500, PDI:1.04) (named as PS-OH), alpha hydroxy omega tempo moiety polystyrene-random-polymethylmethacrylate (Mn=11000, Mw/Mn=1.25) (named as OH tempo PS-r-PMMA) and polystyrene-random-polymethylmethacrylate (PS-r-PMMA) with total molecular weight 15600 and 55 mole% PS (named as PS156) were taken as brush polymer to neutralize the surface energy of substrate. The brush layer was spin coated using 2000 rpm on cleaned Si and afterwards annealing was performed in a muffle furnace (KSL1100X) inside a nitrogen filled glove box at 172 ^{o}C for 72 hrs to allow the polymer chain ends to diffuse and react with the substrate surface. Following that, the annealed layer was toluene rinsed three times to remove the unreacted brush layer from the substrate. The resulting film had thickness of ~5nm. To study the effect of brush layer on BCP morphology evolution, BCP solutions of 1 Wt.% were spin casted using 2500 rpm followed by annealing at 180 ^{o}C for 24 hrs. in the muffle furnace

(KSL1100X) inside a nitrogen filled glove box to allow microphase separation for both PS52 and PMMA22.

A3. Effect of BCP film thickness. In this study only PMMA22 BCP was used. OH- tempo PS-r-PMMA was deposited on cleaned Si substrate as brush layer for this experiment as perpendicular orientation of PMMA cylinders were observed using this brush layer in the previous study. The brush layer deposition was done using a 2 Wt.% solution and 2000 rpm angular speed same way as described in section A2. BCP thickness was varied by varying the spin coating speed. PMMA22 solution (18 mg in 2 ml toluene ,1 Wt. %) spun casted on the brush layer coated substrate with different angular velocity 2000, 2500, 3000 and 4000 RPM for 40s to get variation in BCP film thickness. After deposition, the samples were annealed at 180 for 24 hrs in the muffle furnace (KSL1100X) inside a nitrogen filled glove box to allow microphase separation.

A4. Effect of BCP film annealing time and temperature. PMMA22 BCP of 1 Wt. % solution was used to study the effect of annealing time and temperature. OH-tempo PS-r-PMMA was used as brush layer, and was deposited and grafted to substrate using same method as described in the effect of BCP film thickness section. In the next step, the BCP film was spin casted using 2500 rpm on the brush layer. To study the annealing temperature and time effect the BCP films were annealed at 180 ^{o}C for 2.5 hrs, 12 hrs, 24 hrs and 36 hrs, and 250 ^{o}C for 30 mints, 2.5 hrs, 12 hrs and 24 hrs.

Characterization techniques

Field emission scanning electron microscopy (FESEM-Quanta200) was used for imaging and morphology analysis of BCP nanostructure. BCP and brush layer film

thickness were measured by Filmetrics F50-UVX Film Thickness mapper. BCP microdomain size, inter domain distance was analyzed by ImageJ software.

Results and discussion

B1. Effect of different brush polymers. PS-OH and PS156 were used as brush layer for PS52 BCP, and PS-OH and OH tempo PS-r-PMMA were used as brush layer for PMMA22 BCP deposition. As shown in figure 7(a) and (b) show the SEM images of PS52 a PS cylinder forming BCP after phase separation. Both OH-terminated PS polymer and 55 mole % PS-r-PMMA as brush layer changed the substrate BCP interface and helped the cylinders to orient perpendicularly. In case of PS-OH layer the end OH functional groups graft to the substrate surface and the PS layer forms the wetting layer for preferential PS perpendicular orientation in PS52 [10,11].

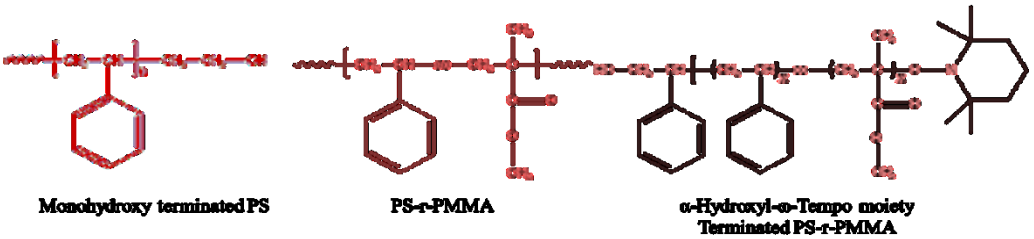

Figure 6. Molecular representation of three different brush polymers used in this study

Whereas in case of PS152 the 55 mole% of PS in the PS-r-PMMA gave a PS preferential wetting layer promoting the perpendicular orientation of PS cylinders in PMMA matrix. However, it is noted that, the sample with PS-OH brush layer was more defect free in the form of perpendicular cylinders as shown in figure 7 (a), whereas the PS-r-PMMA brush layered sample shows some defects in the form of parallel or touching cylinders in places as shown in figure 7(b). In the subsequent experiment it is shown that

the brush layer PS152 with higher PS mole% (55 mole%) when used for PMMA22 BCP didn't quite promote the PMMA cylinder perpendicular orientation as shown in Fig. 7 (c). whereas the PS-r-PMMA brush layered sample shows some defects in the form of parallel lamellae as shown in figure 7(b). In the subsequent experiment it is shown that the brush layer PS152 with higher PS mole% (55 mole. %) when used for PMMA22 BCP didn't quite promote the PMMA lamellae perpendicular orientation as shown in figure 7 (c). For PMMA22 BCP with PS152 mostly islands were formed. In case of PMMA22 BCP the third polymer OH tempo PS-r-PMMA when used as brush layer promoted the PMMA cylinders to orient perpendicularly as shown in Fig 7 (d). In case of OH-tempo PS-r-PMMA, the OH groups are expected to graft on the oxide substrate whereas the tempo group attached to the PMMA (as shown in Fig. 6) stays towards the BCP layer interface, and promotes PMMA cylinders to orient perpendicularly.

B2. Effect of BCP film thickness. In this work, the morphology variation with the BCP thickness variation is shown with the PMMA cylinder forming BCP (PMMA22) used for studying effect of brush layer. In this experiment, OH tempo PS-r-PMMA was used as the brush layer which gave perpendicular orientation in section B1. The BCP film thicknesses were varied by varying the spin coating angular velocity keeping all other experimental conditions same as the conditions mentioned in the section B1 for obtaining perpendicular cylinders of PMMA22. The thicknesses of BCP films measured were ~18 nm, ~29nm, ~42nm and ~53nm with spin coater angular velocity of 4000rpm, 3000rpm, 2500rpm and 2000rpm, respectively. The PMMA cylinders domain size (center to center distance) and the average diameter noted from the Gaussian fitting of the histogram plot are ~40 nm and ~18nm, respectively, as shown in figure 9 (a) & (b). The plot in figure 9

was done from SEM image of the cylindrical PMMA sample shown in figure 8 (b). The perpendicular orientation of PMMA cylinders was observed with the thicknesses (t) of BCP films t~42nm (2500 rpm velocity and 1.05L_0 or ~L_0) and t~18nm (4000 rpm velocity and 0.45L0 or ~1/2 L_0) and lies within the window of PMMA cylinder domain size and half of domain size (L_0 ~ 40nm & L_0/2 ~20nm) as shown in figure 8 (b) and (d), respectively. figure 8 (c) shows the parallel cylinders (lamellar structure) were obtained with the spin coating velocity 3000 rpm, and thickness ~ 29nm (~3/4L_o/~0.75 L_o), which is consistent with the literature report [12–14, 20, 28]. As for the samples with thicknesses 53nm (1.3L_o), mixed parallel and perpendicular morphologies were obtained shown in figure 8 (a).

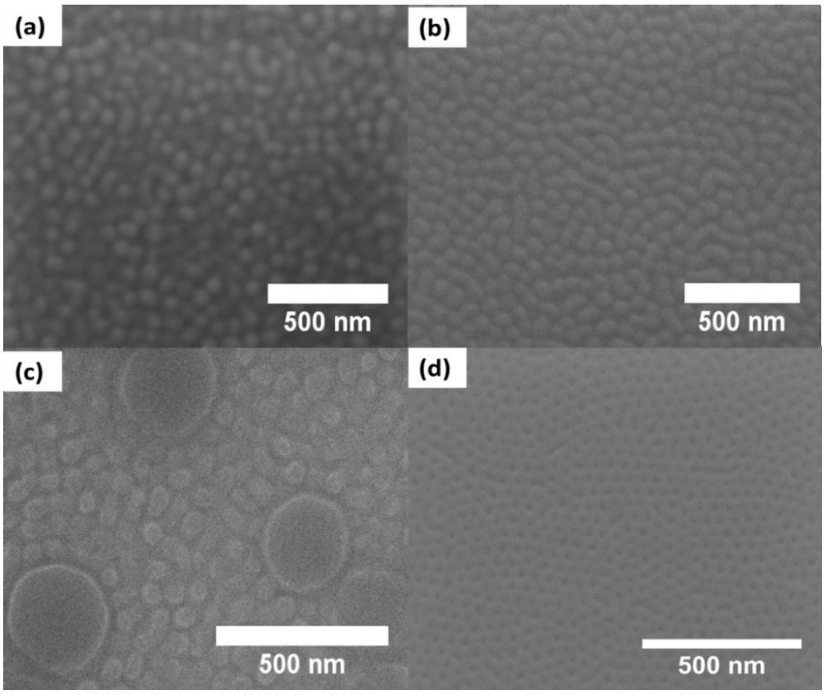

Figure 7. SEM images showing change in BCP thin film morphology with different brush layer (a) PS52 on PS-OH (b) PS52 on PS156 (c) PMMA22 on PS-OH, and (d) PMMA22 on OH tempo PS-r-PMMA

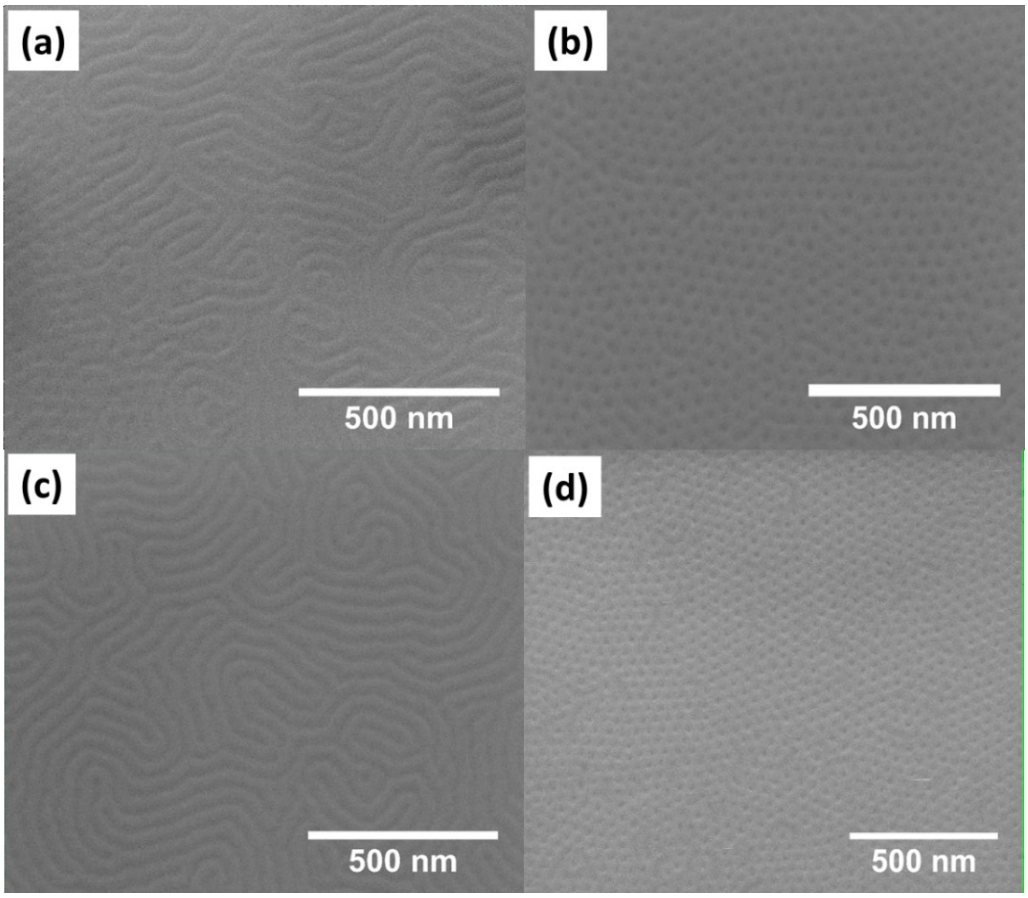

Figure 8. SEM images showing change in BCP morphology of PMMA22 BCP with decrease in film thickness a) 1.3L0 (~53nm) b) 1.05L0 (~42nm) c) 0.75L0 (~29nm) and d) 0.45L0 (~18 nm))

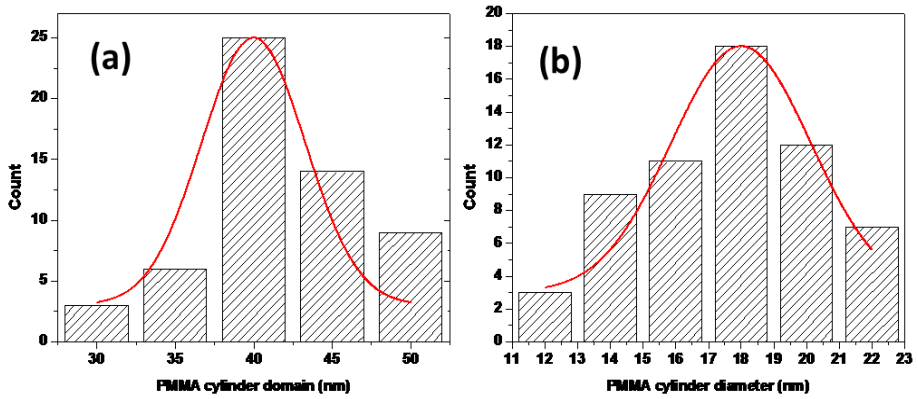

Figure 9. Histogram plotted from Fig.8(b) with Gaussian fitting for a) PMMA cylinder size b) Distance between PMMA Cylinder.

B3. Effect of BCP film annealing time and temperature. The difference in surface energy between PS and PMMA at the surface can be tuned and balanced by varying annealing time and temperature [26].The segregation factor, flory huygens interaction parameter (λ) between two blocks decreases with the increase in temperature of the BCP system [29]. As the temperature exceeds the glass transition temperature, the chain mobility increases, eventually the microdomain arrange themselves in particular fashion.

Dewetting occurs as a result of higher surface energy of BCP compared to the substrate. In this study, the PMMA22 BCP was used; in the deposition process, BCP deposition was done using 2500rpm and BCP film annealing time and temperature were varied keeping all other conditions same as section B1 and B2. Annealing temperatures of 180 ^{o}C was used for 2.5, 12, 24 and 36 hours, and 250 ^{o}C was used for 30 mins, 2.5 hrs 12hrs and 24 hrs. With increasing temperature and time of annealing should be less to optimize the surface energy of two blocks and surface energy between the blocks and substrate for microphase separation. In the first study at 180 ^{o}C for 12 hrs annealing the microphase separation resulted only few perpendicularly oriented cylinders spread randomly at different parts as shown in figure 10(a). It can be attributed due to supplied amount of energy for proper chain mobility is not optimum for complete phase separation throughout the film. As annealing time increased to 24 hrs, morphology conversed into PMMA vertical cylinder only structures, as shown in figure 10 (b). At 36 hrs some defect start to appear in terms of horizontal/parallel cylinders mixed with vertical/perpendicular cylinders, indicating conversion of perpendicular cylinders into parallel/horizontal cylinders with increasing time in agreement with other studies [15, 16]. The small

difference in surface tension between PS and PMMA facilitates the appearance of vertical orientation in the beginning; eventually this small difference is partially responsible for parallel/horizontal orientation with annealing time or in other word with increasing energy by equating the surface energy [22,26]. The same trend was observed for sample treated at higher temperature of 250 ºC, for different times.

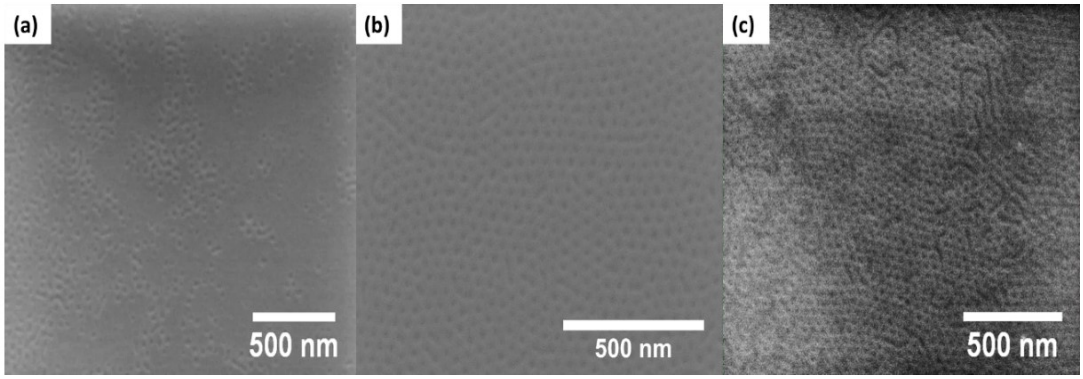

Figure 10. SEM images showing change in BCP morphology of PMMA22 BCP with annealing at 180ºC for a) 12 hrs b) 24 hrs, and C) 36 hrs

To show that both temperature and time have influence on the phase separation and orientation, in the second experiment of this study samples were prepared at 180 ºC 2.5 hrs and 250 ºC 2.5 hrs. The SEM images in figure 11 shows, the phase separation just started at 180 ºC 2.5 hrs timeline as seen from the indistinct structures at figure 11 (a); whereas a parallel cylinder was formed for the 250 ºC 2.5 hrs sample as shown in figure 11 (b). The formation of parallel cylinders in patches or formation of islands is probably due to the modification of brush layer beneath the BCP layer at relatively high temperature as observed by others as well [27]. Further experiments at 250ºC for 30 minutes, 2.5 hrs, 12 hrs and 36 hrs were performed to see the higher temperature effect at different times. Figure 12(a) shows at 250 ºC 30 mints no phase separation can be seen indicating the time is not enough for the threshold of the phase separation to start in this

case. For annealing at 250 ^{o}C 2.5 hrs, 12 hrs and 24 hrs discontinuous films of parallel cylinders are observed (shown in figure 12 (b), (c) and (d), respectively) most probably due to the degradation of the random copolymers in the brush layer at higher temperature as stated above. While comparing the orientation at two different temperatures it is shown that, for 250 ^{o}C temperature, time as low as 2.5 hrs (figure 12 (b)) is enough for obtaining the parallel morphology which is expected to appear post the perpendicular morphology appearance while annealing; whereas for 180 ^{o}C mixed parallel and perpendicular structures were observed (figure 10 (c)) after 36 hrs anneal, and perpendicular cylinders were observed until 24 hrs annealing (figure 10 (a) & (b)). This results at different temperatures and times of annealing clearly show the importance of external thermal energy to modulate the surface energy and as a result formation of parallel or perpendicular orientation of PMMA cylinders.

In summary, the conditions which gave the perpendicular orientation of PMMA22 BCP are listed below:

Deposition parameter	Name and value used
Brush layer polymer name	Alpha hydroxy omega tempo moiety polystyrene random-polymethylmethacrylate
Brush layer weight % in solution	2 wt%
Brush layer annealing temperature and time	172^{0}C 72hrs
BCP weight %	1 wt %
BCP spin coating velocity	2500 and 4000 rpm (thickness -42nm and 29nm)
BCP annealing time and temperature	24 hrs at 180^{0}C

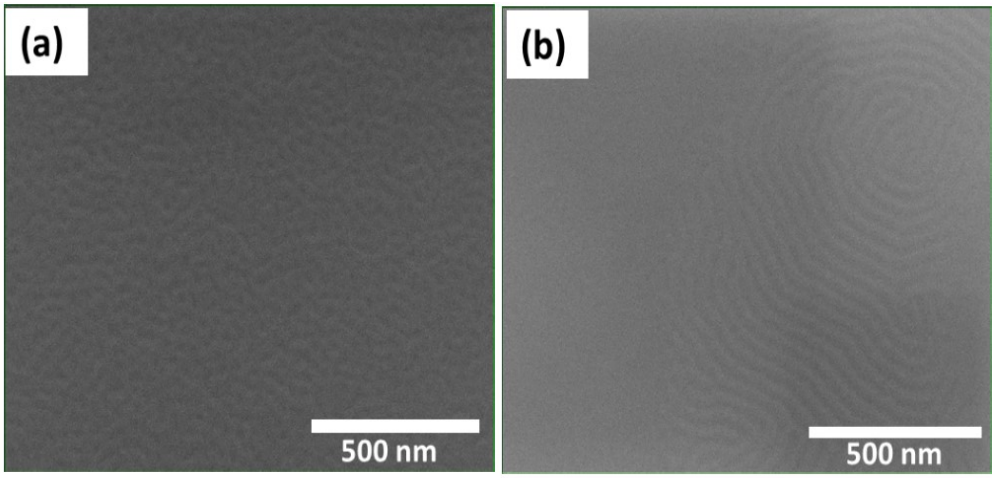

Figure 11. SEM images to show annealing temperature effect on PMMA22 BCP using same annealing time of 2.5 hrs a) 180ºC for 2.5 hrs b) 250ºC for 2.5 hrs

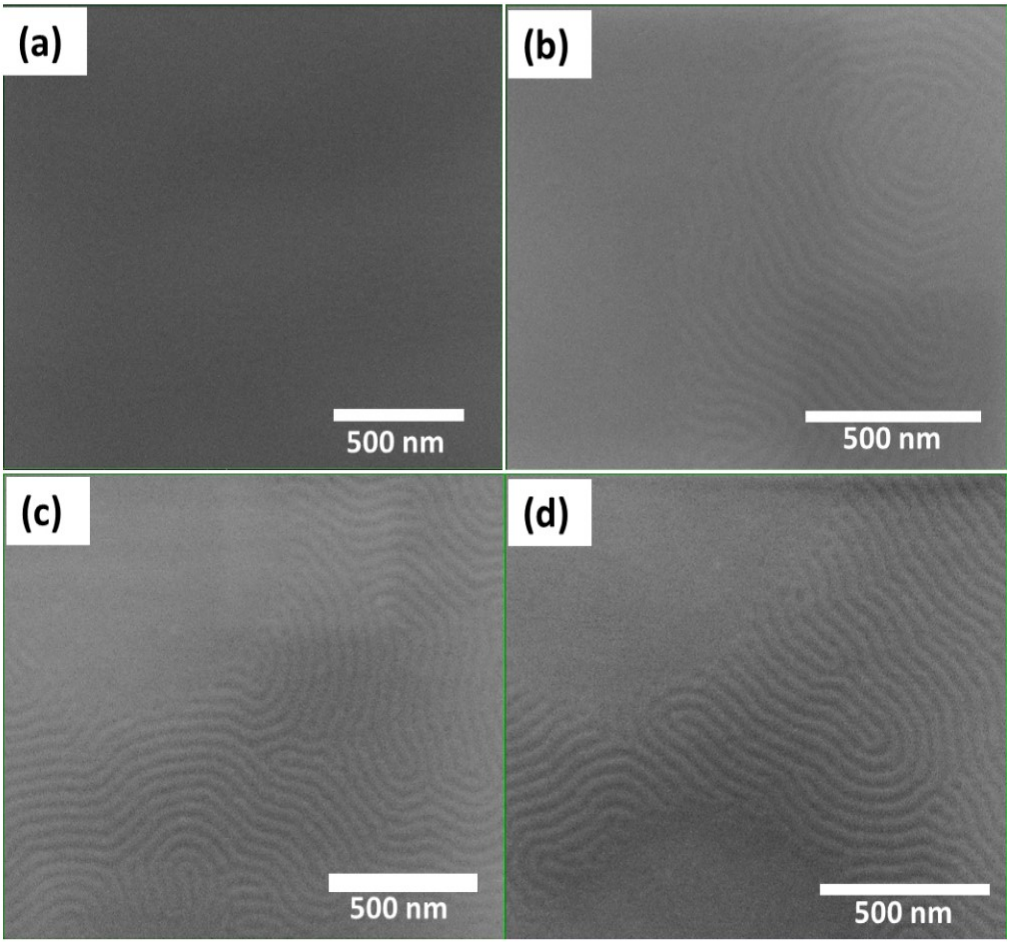

Figure 12. SEM images showing change in BCP morphology of PMMA22 BCP with annealing at 250oC for (a) 30 mints, (b) 2.5 hrs, (c) 12 hrs and (d) 24 hrs

Conclusion

A systematic study of BCP morphology evolution by changing different parameters was performed in this work. Cylinder forming PS-b-PMMA BCPs were used to study the effect of three external experimental parameters on the orientation of the cylinders. In the first study, different brush polymers were selected and studied for two different BCPs to show the proper polymer for perpendicular orientation. It is shown that perpendicular orientation depends on the preferential wetting layer between substrate BCP interface and largely depend on proper selection of brush molecule with respect to the BCP molecule. In the second study, it is shown that with the variation in BCP film thickness perpendicular and parallel orientations were observed only with BCP thicknesses lies within a particular domain size multiple. The third study shows the influence of different annealing times and temperatures on the orientation and formation of BCP microdomain. It is shown that, the temperature and time of annealing need to be optimized for obtaining perpendicular orientation. With too low temperature and less time the energy is not sufficient to promote chain mobility and subsequent microphase separation; whereas with too high temperature and more time the BCP phase separated nanostructures orient in parallel/horizontal/equilibrium orientation due to equal surface energy between two blocks.

References

[1] Y. C. Tseng and S. B. Darling, "Block copolymer nanostructures for technology," *Polymers*, vol. 2, no. 4. pp. 470–489, 2010.

[2] M.-L. Wu and D. Wang, "Microdomain orientation control of PS-b-PMMA films enabled by wettability relay of graphene," *RSC Adv.*, vol. 6, pp. 7527–7531, 2016.

[3] P. Alexandridis and B. Lindman, *Amphiphilic Block Copolymers: Self-Assembly and Applications*. Elsevier Science, 2000.

[4] L. Zhang and A. Eisenberg, "Multiple Morphologies of 'Crew-Cut' Aggregates of Polystyrene-b-poly (acrylic acid) Block Copolymers," *Science (80-).*, vol. 268, no. 5218, pp. 1728–1731, 1995.

[5] S. B. Darling, "Directing the self-assembly of block copolymers," *Progress in Polymer Science (Oxford)*, vol. 32, no. 10. pp. 1152–1204, 2007.

[6] M. Luo and T. H. Epps, "Directed block copolymer thin film self-assembly: Emerging trends in nanopattern fabrication," *Macromolecules*, vol. 46, no. 19. pp. 7567–7579, 2013.

[7] W. Li and M. Müller, "Defects in the Self-Assembly of Block Copolymers and Their Relevance for Directed Self-Assembly," *Annu. Rev. Chem. Biomol. Eng.*, vol. 6, no. 1, pp. 187–216, 2015.

[8] Y. Mai and A. Eisenberg, "Self-assembly of block copolymerswz," *Chem. Soc. Rev. Chem. Soc. Rev*, vol. 41, no. 41, pp. 5969–5985, 2012.

[9] P. Mansky, Y. Liu, E. Huang, T. P. Russell, and C. Hawker, "Con tro lling Polymer-Surface Interactions with Random Copolymer Brushes," *Science (80-.).*, vol. 25, no. 7, pp. 1458–1460, 1997.

[10] R. Guo, E. Kim, J. Gong, S. Choi, S. Ham, and D. Y. Ryu, "Perpendicular orientation of microdomains in PS-b-PMMA thin films on the PS brushed substrates," *Soft Matter*, vol. 7, no. 15, p. 6920, 2011.

[11] L. Oria, A. Ruiz De Luzuriaga, J. A. Alduncin, and F. Perez-Murano, "Polystyrene as a brush layer for directed self-assembly of block co-polymers," *Microelectron. Eng.*, vol. 110, pp. 234–240, Oct. 2013.

[12] K. W. Guarini, C. T. Black, and S. H. I. Yeung, "Optimization of diblock copolymer thin film self assembly," *Adv. Mater.*, vol. 14, no. 18, pp. 1290–1294, 2002.

[13] U. Jeong *et al.*, "Enhancement in the Orientation of the Microdomain in Block Copolymer Thin Films upon the Addition of Homopolymer," *Adv. Mater.*, vol. 16, no. 6, pp. 533–536, 2004.

[14] I. A. Zucchi, E. Poliani, and M. Perego, "Microdomain orientation dependence on thickness in thin films of cylinder-forming PS- b -PMMA," *Nanotechnology*, vol. 21, no. 18, p. 185304, 2010.

[15] P. W. Majewski and K. G. Yager, "Millisecond Ordering of Block Copolymer Films via Photothermal Gradients," *ACS Nano*, vol. 9, no. 4, pp. 3896–3906, 2015.

[16] P. W. Majewski *et al.*, "Reordering transitions during annealing of block copolymer cylinder phases," *Soft Matter*, vol. 12, no. 1, pp. 281–294, 2016.

[17] D. Y. Ryu, "A Generalized Approach to the Modification of Solid Surfaces," *Science (80-).*, vol. 308, no. 5719, pp. 236–239, 2005.

[18] X. Yu, J. Peng, L. Cui, H. Wang, B. Li, and Y. Han, "Morphology Development Of Ultrathin Symmetric Diblock Copolymer Film Via Solvent Vapor Treatment," *Macromolecules*, vol. 37, no. 19, pp. 7301–7307, 2004.

[19] T. Xu *et al.*, "Block copolymer surface reconstruction: A reversible route to nanoporous films," *Adv. Funct. Mater.*, vol. 13, no. 9, pp. 698–702, 2003.

[20] K. W. Guarini, C. T. Black, K. R. Milkove, and R. L. Sandstrom, "Nanoscale patterning using self-assembled polymers for semiconductor applications," *J. Vac. Sci. Technol. B Microelectron. Nanom. Struct.*, vol. 19, no. 6, p. 2784, 2001.

[21] T. Thurn-Albrecht *et al.*, "Nanoscopic templates from oriented block copolymer films," *Adv. Mater.*, vol. 12, no. 11, pp. 787–791, 2000.

[22] E. Han, K. O. Stuen, M. Leolukman, C. C. Liu, P. F. Nealey, and P. Gopalan, "Perpendicular orientation of domains in cylinder-forming block copolymer thick films by controlled interfacial interactions," *Macromolecules*, vol. 42, no. 13, pp. 4896–4901, 2009.

[23] R. Zhang, "Dynamic Temperature Gradient Directed Self-assembly Of Block Copolymer/Nanoparticle Thin Films," The University of Akron, 2013.

[24] R. Farrell, T. G. Fitzgerald, D. Borah, J. D. Holmes, and M. Morris, "Chemical interactions and their role in the microphase separation of block copolymer thin films.," *International journal of molecular sciences*, vol. 10, no. 9, pp. 3671–712, 2009.

[25] M. J. Pavan and R. Shenhar, "Two-dimensional nanoparticle organization using block copolymer thin films as templates," *J. Mater. Chem.*, vol. 21, no. 7, pp. 2028–2040, 2011.

[26] P. Mansky, T. Russell, C. Hawker, J. Mays, D. Cook, and S. Satija, "Interfacial Segregation in Disordered Block Copolymers: Effect of Tunable Surface Potentials," *Phys. Rev. Lett.*, vol. 79, no. 2, pp. 237–240, 1997.

[27] V. Gianotti *et al.*, "On the Thermal Stability of PS- *b* -PMMA Block and P(S- *r* -MMA) Random Copolymers for Nanopatterning Applications," *Macromolecules*, vol. 46, no. 20, pp. 8224–8234, 2013.

[28] T. Thurn-Albrecht, J. Derouchey, T. P. Russell, and H. M. Jaeger, "Overcoming Interfacial Interactions With Electric Fields," *Macromolecules*, vol. 33, no. 9, pp. 3250–3253, 2000.

[29] E. Kim, S. Choi, R. Guo, D. Y. Ryu, C. J. Hawker, and T. P. Russell, “Transition behavior of PS-b-PMMA films on the balanced interfacial interactions,” *Polymer (Guildf).*, vol. 51, no. 26, pp. 6313–6318, 2010.

BLOCK COPOLYMER TEMPLATED TiO_2 NANODOTS USING ROOM TEMPERATURE PULSED LASER DEPOSITION

Abstract

Block copolymer (BCP) templated inorganic material nanopatterning often termed as BCP lithography has received significant attention recently as it's self-assembly property offers different morphology of nanostructures. The BCP lithography method which is a combination of self-assembled BCP nanostructures fabrication and inorganic material deposition requires a low temperature inorganic deposition process to avoid polymer degradation. In this regard, there are only few methods like sol-gel deposition and atomic layer deposition to synthesize superior quality metal oxides and metals at low temperature. In this paper, we are reporting a novel method combining BCP template and room temperature pulsed laser deposition (PLD) to synthesize TiO_2 nanodot films. This BCP templated TiO_2 nanodots maintain the morphology of the template; which is a promising result for using this method to explore other self-assembled morphologies. Energy dispersive x-ray spectroscopy (EDX) confirms the presence of Ti and O_2 in the nanodot films, and x-ray diffraction (XRD) data shows mixture of both anatase and rutile TiO_2 crystalline phase. The photoluminescence (PL) spectrum for the synthesize TiO_2 is dominated by a broad peak extending from visible to near infrared (NIR), which consists of characteristic peaks for TiO_2 anatase (visible) and rutile phase (NIR). The fabricated closely-packed well-ordered TiO_2 nanodot films will be attractive for different optoelectronics, sensing and catalysis applications. This fabrication method combining BCP and PLD has been explored only in few works so far, and is expected to

give a promising method to synthesize highly ordered nanostructures of different morphologies, and of different materials.

Introduction

Well-ordered low dimensional nanostructures are gaining significant attention because of their unique optical, electrical, magnetic and chemical properties in advanced technological field[1]. The properties of these structures usually depend on their shape, size, arrangements and overall material quality. There are several bottom up approaches for nanofabrication to perform the direct synthesis of nanostructures at the atomic or molecular level, such as various vapor deposition methods (e.g. atomic layer deposition (ALD), pulsed laser deposition (PLD) & chemical vapor deposition (CVD)), and chemical solution process etc.[2–5]. Although nanostructures grown using these methods show good structural, electrical and optical properties, in practice these methods are not yet self-sufficient enough to produce reproducible, well-ordered and large area patterns for devices. In this field of research, self-assembled materials for direct synthesis of nanostructures or as templates have received significant attention in the industry for well-ordered and wide area patterning; especially the use of block copolymers (BCPs) material is advancing remarkably to provide the microelectronic and optoelectronic industry a new method for low dimension and well-ordered patterning technology[6,7]. BCPs self-assemble into a range of morphologies like lamellar, cylindrical and spherical that makes it suitable candidates for two and three dimensional lithographic processes [7–9]. Subsequent deposition of inorganic materials in these nanostructured BCP films leads to formation of similar morphology of inorganic nanostructures. By varying parameters like

molecular ratio and volume fraction of BCP during synthesis, the shape and size of nanopattern can be tuned [6,10].

Titanium dioxide (TiO_2) is a highly promising semiconductor material because of its large band gap, high refractive index, high dielectric constant and high surface-activity [11]. The unique structural and functional properties of TiO_2 is very attractive in the area like photo catalysis, water splitting, solar cells, super capacitors and lithium-ion batteries [12–14]. Controlled nanostructures of TiO_2 is even more attractive because of their improved optical and electrical properties such as high surface to volume ratio and conductivity compared to bulk [13,15,16]. In this regard highly ordered, and superior quality TiO_2 materials are important criteria for the future optoelectronics and energy industry to thrive.

In this paper, a novel approach to fabricate aligned TiO_2 nanodots using BCP cylindrical nanostructures as template is presented. The PLD method at room temperature has been used as inorganic deposition method to fabricate the TiO_2 nanodots. The PLD technique provides deposition of high quality films and coating of TiO_2 with excellent adhesive strength [17]. Although a high temperature PLD deposition method is usually used for depositing crystalline TiO_2 films [17] in this work we have adopted room temperature PLD method to avoid any degradation of BCP template. The PLD deposited TiO_2 on BCP was further annealed in high temperature to remove the sacrificial polymers and make the as deposited amorphous TiO_2 crystalline. To our knowledge, there are reports on fabrication of different TiO_2 nanostructures using other inorganic oxide deposition methods in conjunction with BCP template [18,19]; and only one report on BCP assisted PLD method for fabrication of lead titanate ($PbTiO_3$) nanostructures [20].

This unique method of BCP assisted PLD grown TiO_2 nanodots will open up new avenues of fabrication using many other morphologies available from BCPs and other inorganic materials possible to deposit by PLD method. Field emission scanning electron microscopy (FESEM) and atomic force microscopy (AFM) were used for microscopic imaging of the nanostructures, energy dispersive x-ray spectroscopy (EDX) and x-ray diffraction (XRD) data were used to evaluate the TiO_2 nanodots structural property, and photoluminescence (PL) spectroscopy was done for investigating the optical property of these nanodots.

Experiments

BCP nanostructures fabrication. Si wafers with thin layer of native oxide were used as substrates in this work. The substrates were cleaned to remove any organic residue on the native oxide layer using hydrogen peroxide (H_2O_2), ammonium hydroxide (NH_4OH) and DI water (H_2O) at 65 ^oC for 2.5 hrs. In this work, to achieve perpendicular orientation of the BCP domains, a brush layer was deposited on the cleaned Si substrate. The orientation of BCP nanostructures leads by the surface energy of the substrate [21]. polystyrene-random-polymethylmethacrylate (PS-r-PMMA) with total molecular weight 156000 and 55 mole% PS was used as brush layer. The brush layer was deposited from 1wt. % toluene solution using spin casting. The layer was annealed at 240^oC on a hot plate inside a nitrogen atmosphere glove box for 40 minutes to graft the brush layer polymer on the substrate surface. The brush layer was then toluene rinsed three times to remove the unreacted layer from the substrate. The BCP used in this study was polystyrene-block-polymethylmethacrylate (PS-b-PMMA) of molecular weight M_w

52000 (PS) and 142000 (PMMA); named here as PS52. The BCP layer was deposited on the bush layer grafted substrate from 1 wt.% toluene solution using a spin coater. The samples, were then annealed in a muffle furnace (MTI Corporation KSL1100X) situated inside the glove box at 180 ºC for 24 hrs to facilitate microphase separation of PS and PMMA domains; which formed PS cylinders in PMMA matrix for this polymer with the above mentioned experimental conditions. All the chemicals were purchased from Sigma Aldrich and the polymers were purchased from Polymer Source Inc.

TiO2 nanostructures deposition. For depositing ordered TiO_2 nanostructures, first PMMA domain was etched selectively from the BCP nanostructured film. It is already shown that PMMA preferably etched compared to PS polymer during oxygen (O_2) plasma etching [22]. In this work, controlled O_2 plasma etching with power 50 W, flow rate 5.68 Sccm and 400 mTorr pressure for 5 Sec was used to etch the PMMA domain selectively. The PLD TiO_2 was expected to get deposited as a thin layer in the etched PMMA domain, as well as on the PS cylinder surface. TiO_2 sputtering target (Kurt J. Lesker) was used for the PLD deposition. At 2×10^{-5} mbar PLD chamber pressure a beam of nanosecond pulse laser using a 248 nm UV excimer laser was focused onto the target; the laser beam used in this work, with 1.2 J/cm^2 energy density and 1mm spot diameter was fallen on the TiO_2 target and the evaporated plasma plume deposited on the surface of the PMMA etched BCP nanostructures sample placed at room temperature. The TiO_2 target was fixed with an electric motor inside the PLD chamber to avoid the deposition of material only at particular spot on substrate. The distance between samples to target was 4.5 cm. A range of laser pulse shots were used in this work such as 3000, 6000, 9000 and 12000 to observe any difference in nanostructure formation; in this paper

all the data shown are for samples deposited with 6000 laser pulse shots only. The PLD deposition conditions are summarized below.

PLD deposition parameters	Value used
Chamber pressure	2×10^{-5}
Growth temperature	22^0C
Laser energy density	1.2j/cm^2
Sample-target distance	45mm
Pulse shots used	3000,6000,9000,12000
Laser wavelength	266nm
Spot size	1mm diameter

Following the deposition, the samples were annealed into a furnace (MTI corporation MTI 11000 X) at 500 ºC for 7hrs in air; to remove any remaining polymers and to transform the amorphous TiO_2 into crystal. This high temperature annealing step also promotes the formation of TiO_2 nanodots around the PS cylinders from the thin continuous layer of TiO2.

Characterizations

Field Emission Scanning Electron Microscope (FESEM-Quanta 200) was used to do the imaging of BCP and TiO2 nanostructures samples. The elemental analysis of the TiO_2 nanostructures samples were done with the help of SEM energy dispersive X-ray spectroscopy (EDX) by using a field emission gun (Oxford Instruments) attached to the FESEM system. Surface morphology of the nanodot films were investigated using an

atomic force microscope (Bruker-Dimension Icon). The AFM done using 8 nm TESP Si tip in tapping mode. The AFM data were processed using Bruker NanoScope Analysis Suite 1.30 software. X-ray diffraction (XRD) measurements were done using a Bruker D8 Discover instrument operating at 40 kV and 40 mA. The XRD instrument with a characteristic X-ray source of Cu tube (Cu Kα, λ= 1.54184 Å) was used. The PL measurements were done with a Horiba Labram HR Raman-PL system using 325 nm He-Cd laser.

Results and Discussion

The schematic diagram for the whole procedure to fabricate TiO_2 nanodots using BCP lithography and PLD method is shown in figure 13. The diagram shows the procedure steps which are briefly- (i) BCP nanostructures fabrication steps, (ii) BCP template formation, (iii) PLD deposition and (iv) polymer removal to obtain the TiO2 only nanodot structures.

Figure 14 (a) shows the SEM image of the as grown microphase separated PS52 without any further treatment for imaging. A brush layer of PS-r-PMMA was used to facilitate the growth of vertical cylinder formation; a well-known fact in the BCP research[21]. Following the BCP film casting on brush layered substrate temperature annealing was done to promote the microphase separation of the domains; which gives a periodic arrangement of vertical cylindrical nanostructures in this case. The cylinder diameter and the domain size/cylinder to cylinder distance are shown in figure 14(b) ad (c) using the histogram plots. It is noted from the Gaussian curve fitting (figure 14 (b) &

(c) red curves) that, the average diameter of the cylinders is ~58 nm, and the average domain size of the cylinders are ~80 nm.

In this work, the BCP cylindrical nanostructures were used as a template for TiO_2 nanostructure fabrication. To this end, O_2 plasma etching was performed on the as grown BCP samples to etch one domain selectively; which is PMMA in this case. Although it is expected that PMMA preferentially etches to PS, but there might be some residual PMMA and some of the PS polymer may get etched in the process due to the proximity of the etching rate for these two polymers. Figure 15 shows SEM images at different

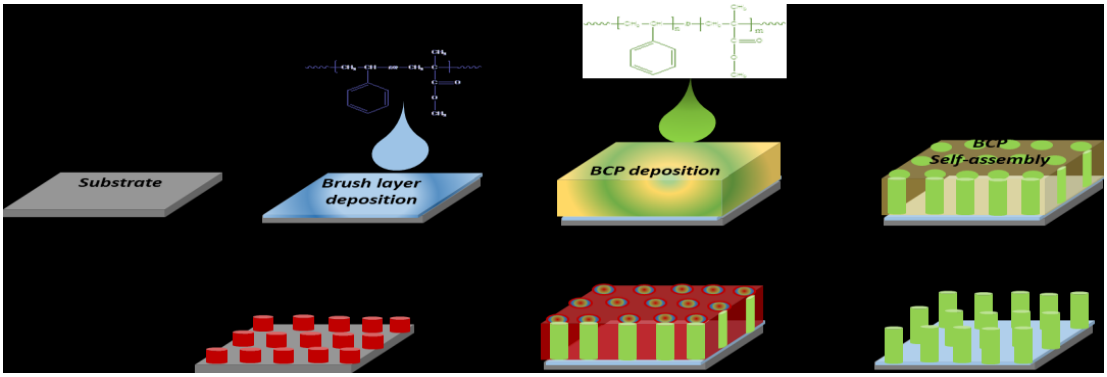

Figure 13. Schematic Diagram of the TiO2 nanodots fabrication procedure using BCP template assisted PLD deposition method

stages of fabrication. Figure 15(a) and (b) show the SEM images of as grown PS-b-PMMA nanocylinder sample and the same sample after PMMA etching, respectively. The PMMA etched sample was used as BCP template for PLD deposition of TiO_2 nanostructures. The substrate was held in room temperature to avoid any degradation of polymer template; which leads to formation of amorphous TiO_2 thin layer. The amorphous TiO_2 deposited sample was then annealed at 500 ^oC for 7 hrs in air for the formation of crystalline TiO_2 and etching the polymers in the same step. Figure 15 (c)

shows the SEM image of the same sample used in Figure 15(a) & (b) after PLD deposition and temperature annealing. As mentioned in abo, no. of pulse shots which deposits different thicknesses of thin films were varied (3000, 6000, 9000 &12000) to observe any difference in the TiO_2 nanodot formation. No significant difference was observed in the nanodot formation due to the variation of pulse shots in that range (data not shown). In this report, all the data shown were measured on samples made with 6000 PLD pulse shots.

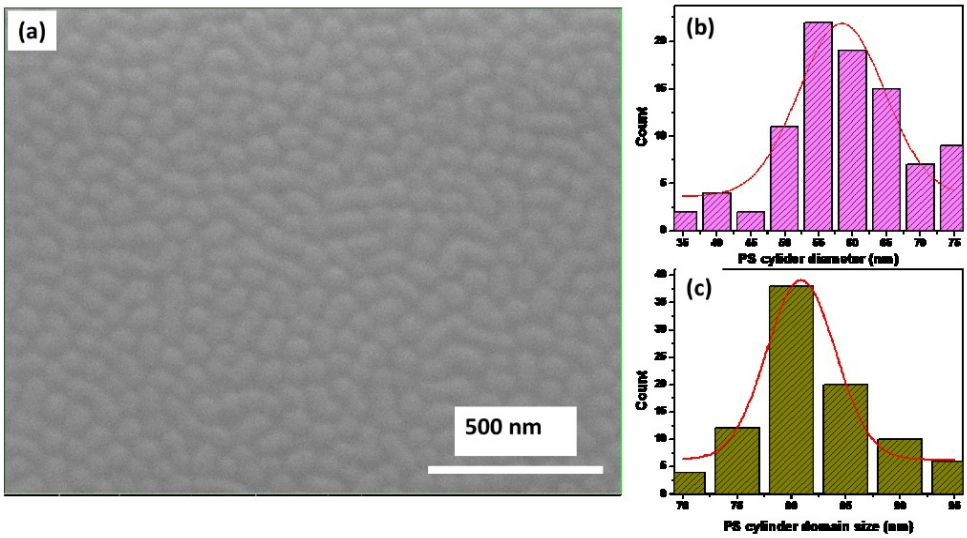

Figure 14. a) SEM image of as grown PS-b-PMMA BCP (PS52). Histogram plots for PS cylinder (a) diameter (average ~58 nm) and (b) domain distance (average ~80 nm).

Figure 16 shows the SEM and AFM images of the TiO2 nanodots only sample and corresponding nanodot size and domain calculation from these images. From the low magnification image shown in figure 16 (a) it is observed that, the nanodot formation is very uniform throughout the sample and it was consistent for all the samples grown in this study. Figure 16 (b) & (c) show the histogram plots for the nanodot diameter and domain size, respectively derived from the SEM image. From the Gaussian fitting of the

plot (Fig. 16(b) & (c) red curves) the average diameter and domain size was noted as ~75 nm and ~40 nm, respectively. Figure 16(d) is the AFM topographical image of the same sample and Figure 16(e) is the 3D projection of image 16(d). The average height of the nanodots are ~10 nm, calculated from depth histogram of the topographical image (Fig. 16(d)) using Bruker NanoScope Analysis Suite 1.30 (plot not shown). The average

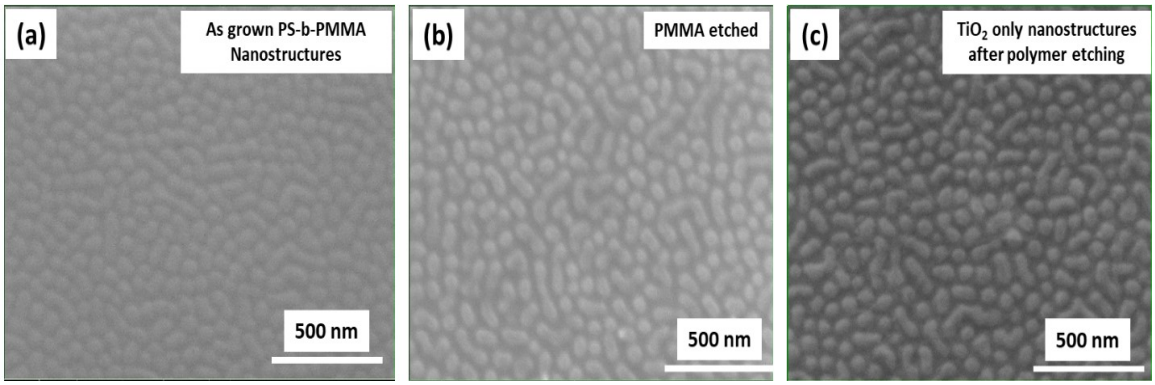

Figure 15. SEM images at different stage of fabrication of TiO2 Nanodots a) as-grown PS-b-PMMA nanostructures after phase separation, (b) PS cylinders after selective PMMA etching from the casted BCP nanostructured film, and (c) TiO2 only nanodots after polymer etching.

diameter of the nanodots calculated from the depth histogram of the AFM image is ~70 nm, which is almost similar to the average diameter value calculated from the SEM. TiO_2 nanodots it is noted that, TiO_2 nanodot diameter was almost same as the PMMA domain size in between the PS cylinders. From this information, the idea behind the TiO_2 nanodot formation was interpreted as- during PLD deposition, small TiO_2 nanoparticles in the form of continuous thin film get deposited on the PMMA etched BCP template; afterwards during high temperature annealing (500 ^oC) and PS cylinder evaporation these TiO_2 nanoparticles nucleated in the void PMMA domain space in between PS cylinders, breaking up the TiO2 thin layer; resulting in formation of TiO2 nanodots.

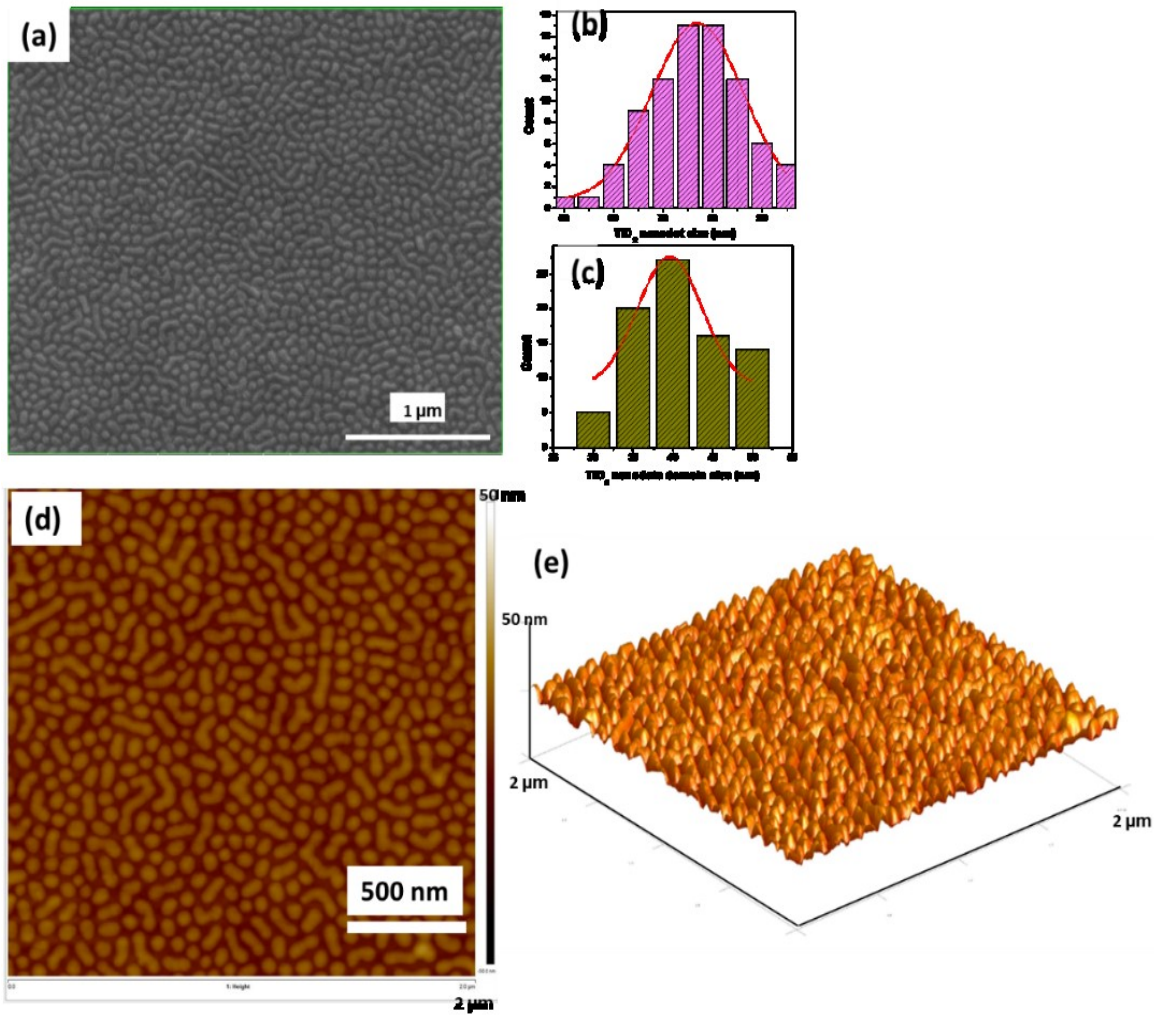

Figure 16.(a) Low magnification SEM image of TiO2 nanodot only sample after polymer removal. (b) and (c) are the histogram plots for the diameter and interdomain distance of the nanodots calculated from the SEM image shown in (a). (d) is the AFM topographical image of the same sample and (e) is the 3D projection of (d)

The elemental analysis was done using EDX spectroscopy attached to the SEM system on the TiO_2 only nanodots to investigate and confirm the TiO_2 deposition. From EDX study, the presence of Ti and O was confirmed as shown in figure 17 (b) & (c). The EDX spectrum is analyzed by the INCA software that runs the EDX detector and determines the atomic percentage of the elements present in the scanned area. Multiple

spots were taken to get an average over the sample for elemental composition. Here one spectrum and corresponding point in the SEM image are shown in figure 17. Figure 17 (b) is the EDX spectrum recorded from the point of interest (indicated as spectrum 1) shown in figure 17 (a). The point of interest was taken exactly on a TiO_2 nanoisland as shown in figure 17(a). The x-ray emission peaks at 0.452 (Ti L line), 4.512 (Ti Kα line), and 0.525 (O Kα line) are shown in the spectrum using corresponding Ti and O balloons (Fig 17 (b)). The most intense x-ray emission ~1.74 KeV (Si Kα line) is from the substrate, and the peak is not shown here to focus the Ti and O peaks in the spectrum. The atomic % for Ti and O are ~15% and ~85%, as shown below figure 17 (b). Please note, the atomic % contribution from Si substrate and carbon was excluded from the calculation; the O contribution in the measurement as shown in the atomic % was coming not only from TiO_2, but also from the substrate native oxide and from the surrounding.

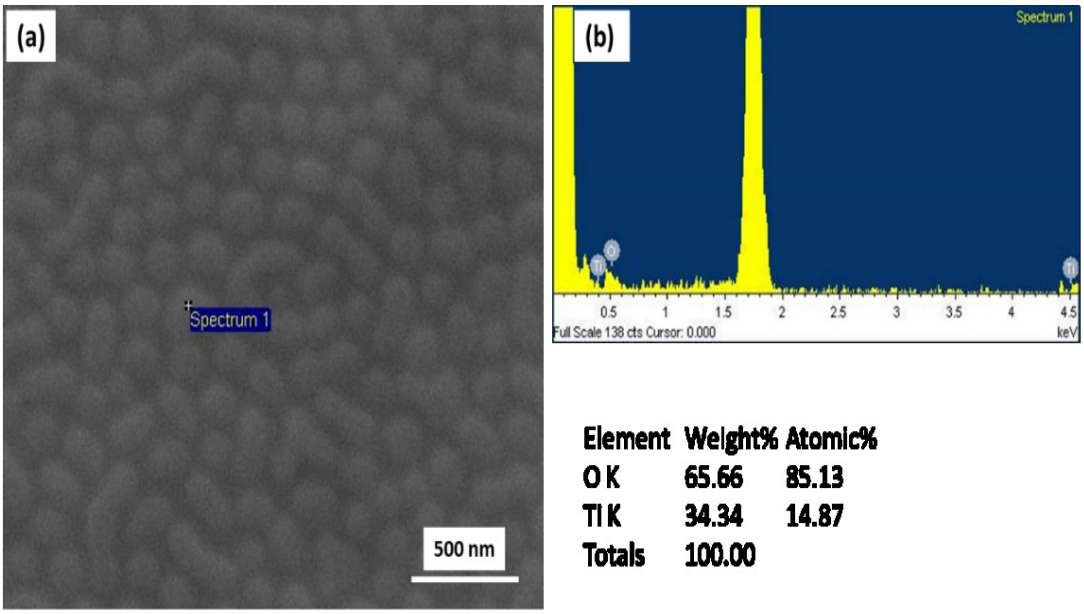

Figure 17. Elemental analysis of TiO2 nanodots using EDX spectrum as shown in (b) and the corresponding SEM image is shown in (a). The point of interest in the SEM image where spectrum was recorded is shown as spectrum 1. The element percentages are shown in (c)

XRD of the TiO_2 nanodot only sample after annealing was done to investigate the structural development of the material. As mentioned before, due to room temperature PLD deposition the as deposited TiO_2 was amorphous in nature. However, after annealing at 500 ºC for 7hrs the resultant TiO_2 nanodots were expected to become crystalline in nature. Figure 18 shows the XRD 2θ plot for the TiO_2 nanodot sample; measurements were done using $CuK_{\alpha 5}$ radiation on x-ray diffractometer. The intensity of TiO_2 peak were very low in comparison to the peak coming from Si substrate. To eliminate the Si peak, the sample was tilted 7.8º using chi rotation. The Bragg's diffraction peaks observed at 27.44º, 44.97º, 54.77º and 56.77º are correspond to TiO_2 rutile phase with *hkl* plane of (110), (210), (211) and (220), respectively [23–25]. The peak at Bragg's angle 38.67º is corresponds to TiO_2 anatase (112) *hkl* plane[23]. It is noted from the XRD data that, the rutile phase of TiO_2 was observed at relatively low annealing temperature of 500 ºC compared to the usual high temperature for stable rutile phase formation[26]. This can be attributed to oxygen deficiency during PLD deposition, which was performed at room temperature under vacuum. Our observation is in agreement with Ishii *et. al.* who has also obtained rutile phase for PLD grown TiO_2 at relatively low annealing temperature [27]. This rutile TiO2 formation at relatively low annealing temperature will be very attractive for optical applications [28,29].

Finally, PL spectroscopy was performed to study the optical properties of these TiO_2 nanodots. The sample used for this study was the same sample shown in figure 15 (c), figure 16 and figure 18. As seen from figure 19 the PL spectrum of the TiO_2 sample is dominated by a broad peak in the visible and near infrared (NIR) region (~1.5-2.6 eV), which consists of the characteristic peaks of TiO_2 anatase phase in the visible region and

TiO_2 rutile phase in the NIR region, as reported by many others [24,30–40]. The broad PL spectrum of anatase TiO_2 in the visible region is attributed to combination of different reasons such as self-trapped excitons, oxygen vacancies and defect sites, impurities or reduced metal ions, etc. [32–37]. The PL spectrum of rutile phase is more difficult to interpret, however there are several reports attributing the NIR region broad peak to interstitial Ti^{3+} ions, trapped holes and free holes etc. in the rutile phase [24, 37–40]. The lack of oxygen during PLD growth in the chamber can be identified as one of the reason in the exhibition of the broad peak seen in Figure 19 due to the formation of oxygen vacancies and Ti interstitials. In addition, this PL spectrum also confirms that the fabricated nanostructures are mixture of two TiO_2 crystalline phases; which is in agreement with the XRD data.

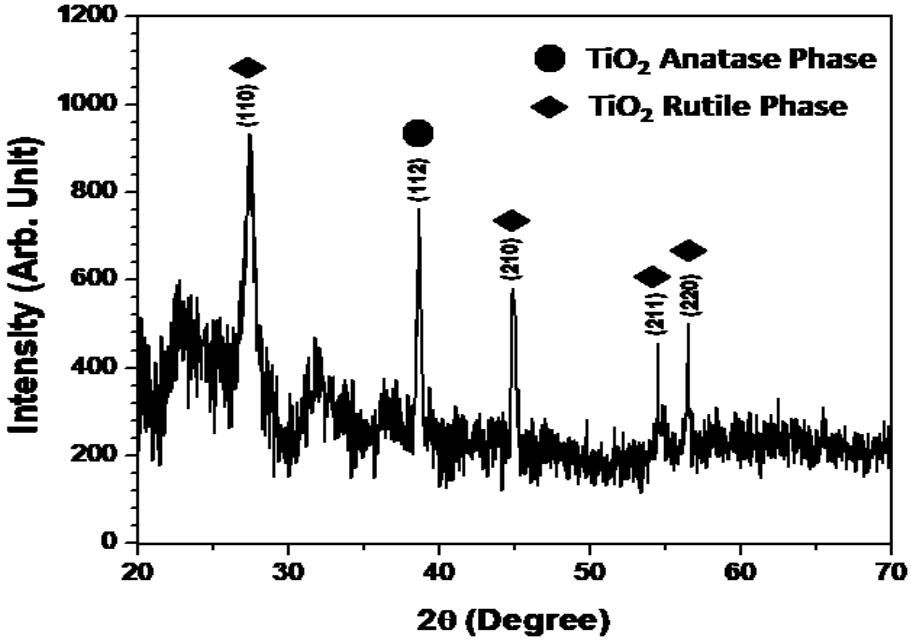

Figure 18. XRD 2θ plot of the TiO2 nanodot only sample as shown in the SEM and AFM image of Fig. 15(c) and Fig. 16 after annealing at 500ºC for 7 hrs. The nanodots exhibit mostly TiO2 rutile phase peaks and one TiO2 anatase phase peak

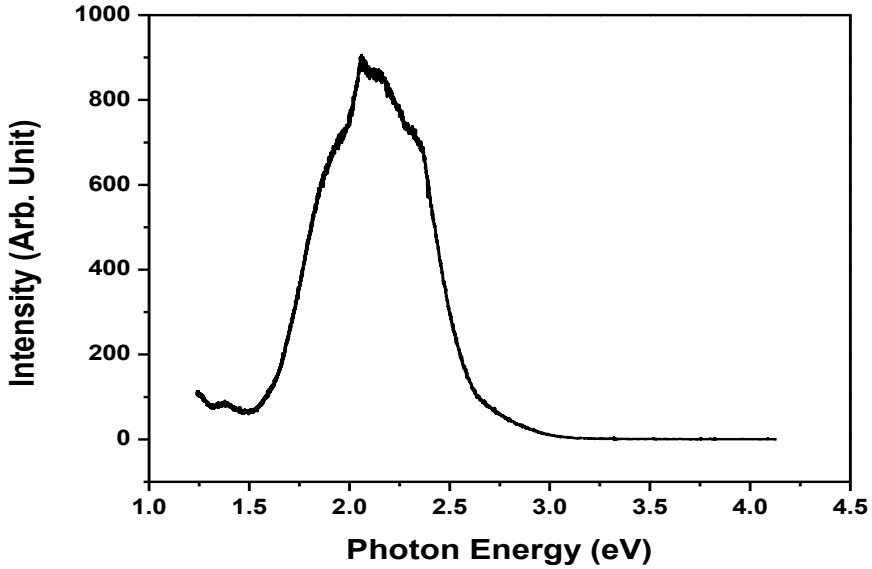

Figure 19. Room temperature PL spectrum of TiO2 nanodot sample showing a broad peak in the visible and NIR region (~1.5-2.6 eV) of the spectrum.

Conclusion

In conclusion, this paper shows a successful demonstration of the fabrication of TiO2 nanodots using BCP as template and room temperature PLD. High temperature annealing of the samples after deposition not only promoted crystallinity of the as-deposited amorphous TiO_2 material, it also helped in the formation of these nanostructures from its thin film form. The proposed hypothesis behind the nanodot formation is, the deposited TiO_2 nanoparticles nucleated in the void PMMA domain space in between PS cylinders during high temperature (500 ^oC) annealing and polymer evaporation, breaking up the TiO_2 layer. The EDX elemental analysis shows the presence of Ti and O atoms. Further the XRD and PL data confirm the presence of mixed phase crystalline TiO_2 material. In addition, the information about TiO_2 crystal planes were obtained from the XRD 2θ scan. The broad PL spectrum shows a broad peak in the

visible and NIR spectral region for the anatase and rutile phase, respectively. The fabrication procedure depicted in this paper will open up new avenue for inorganic nanostructures deposition method with different BCP morphologies and with other inorganic materials possible by PLD method. Apart from demonstrating a novel fabrication method, this paper also shows the formation of stable TiO_2 rutile phase at relatively low temperature, which will be very attractive for many optical applications [28,29].

References

[1] A. Ghicov and P. Schmuki, "Self-ordering electrochemistry: a review on growth and functionality of TiO2nanotubes and other self-aligned MOx structures," *Chem. Commun.*, no. 20, pp. 2791–2808, 2009.

[2] Z. Fan and J. G. Lu, "Zinc Oxide Nanostructures: Synthesis and Properties," *J. Nanosci. Nanotechnol.*, vol. 5, no. 10, pp. 1561–1573, 2005.

[3] M. Knez, K. Nielsch, and L. Niinistö, "Synthesis and Surface Engineering of Complex Nanostructures by Atomic Layer Deposition," *Adv. Mater.*, vol. 19, no. 21, pp. 3425–3438, 2007.

[4] C. N. R. Rao, F. L. Deepak, G. Gundiah, and A. Govindaraj, "Inorganic nanowires," *Prog. Solid State Chem.*, vol. 31, no. 1, pp. 5–147, 2003.

[5] S. C.; Z. H. Singh, "Nanomaterials and Nanopatterns Based on Laser Processing: A Brief Review on Current State of Art," *Sci. Adv. Mater.*, vol. 4, no. 3–4, pp. 368–390, 2012.

[6] C. Park, J. Yoon, and E. L. Thomas, "Enabling nanotechnology with self- assembled block copolymer patterns," *Polymer (Guildf).*, vol. 44, no. 22, pp. 6725–6760, 2003.

[7] Y. C. Tseng and S. B. Darling, "Block copolymer nanostructures for technology," *Polymers*, vol. 2, no. 4. pp. 470–489, 2010.

[8] H.-C. Kim, S.-M. Park, and W. D. Hinsberg, "Block Copolymer Based Nanostructures: Materials, Processes, and Applications to Electronics," *Chem. Rev.*, vol. 110, no. 1, pp. 146–177, 2010.

[9] C. A. Ross, K. K. Berggren, J. Y. Cheng, Y. S. Jung, and J.-B. Chang, "Three-Dimensional Nanofabrication by Block Copolymer Self-Assembly," *Adv. Mater.*, vol. 26, no. 25, pp. 4386–4396, 2014.

[10] A. Nunns, J. Gwyther, and I. Manners, "Inorganic block copolymer lithography," *Polym. (United Kingdom)*, vol. 54, no. 4, pp. 1269–1284, 2013.

[11] G. K. Mor, O. K. Varghese, M. Paulose, K. Shankar, and C. A. Grimes, "A review on highly ordered, vertically oriented TiO2 nanotube arrays: Fabrication, material properties, and solar energy applications," *Sol. Energy Mater. Sol. Cells*, vol. 90, no. 14, pp. 2011–2075, 2006.

[12] S. M. Gupta and M. Tripathi, "A review of TiO2 nanoparticles," *Chinese Sci. Bull.*, vol. 56, no. 16, pp. 1639–1657, 2011.

[13] V. P. Gupta and N. M. Ravindra, "Optoelectronic properties of rutile (TiO2)," *J. Phys. Chem. Solids*, vol. 41, no. 6, pp. 591–594, 1980.

[14] J. Tian, Z. Zhao, A. Kumar, R. I. Boughton, and H. Liu, "Recent progress in design, synthesis and applications of one-dimensional TiO2 nanostructured surface heterostructures: a review," *Chem. Soc. Rev.*, vol. 43, no. 20, pp. 6920–6937, 2014.

[15] B. L. Ellis, P. Knauth, and T. Djenizian, "Three-dimensional self-supported metal oxides for advanced energy storage," *Advanced Materials*, vol. 26, no. 21. pp. 3368–3397, 2014.

[16] A. Fakharuddin *et al.*, "Vertical TiO2 Nanorods as a Medium for Stable and High-Efficiency Perovskite Solar Modules," *ACS Nano*, vol. 9, no. 8, pp. 8420–8429, 2015.

[17] A. Escobar-Alarcon, Haro-Poniatowki,E;Camacho-LOpez, M.A; Fenandez-Guasti,M:Jimenez-Jarquin;Sanchez-pinenda, "Structural Characterization of TiO2 thin films obtained by pulsedlaser deposition," *Appl. Surf. Sci.*, vol. 137, no. 1, pp. 38–44, 1999.

[18] P. S. Chinthamanipeta, Q. Lou, and D. A. Shipp, "Periodic titania nanostructures using block copolymer templates," *ACS Nano*, vol. 5, no. 1, pp. 450–456, 2011.

[19] Y. Yin, J.;Xu,Q.; Wang, "Highly Ordered TiO2 Nanostructures by Sequesntial Vapour Infiltration of Block Copolymer Micellar Films in an Atomic Layer Deposition Reactor," *J. Mater. Chem.*, vol. 1, no. 5, pp. 1029–1036, 2013.

[20] W. Van Zoelen, A. H. G. Vlooswijk, A. Ferri, A. M. Andringa, B. Noheda, and G. Ten Brinke, "Ordered arrays of ferroelectric nanoparticles by pulsed laser deposition on PS-b-P4VP(PDP) supramolecule-based templates," *Chem. Mater.*, vol. 21, no. 19, pp. 4719–4723, 2009.

[21] P. Mansky, Y. Liu, E. Huang, T. P. Russell, and C. Hawker, “Con tro lling Polymer-Surface Interactions with Random Copolymer Brushes,” *Science (80-.).*, vol. 25, no. 7, pp. 1458–1460, 1997.

[22] T. H. Koji Asakawa, “Nanopatterning with Microdomains of Block Copolymers using Reactive-Ion Etching Selectivity Nanopatterning with Microdomains of Block Copolymers using Reactive-Ion Etching Selectivity,” *Jpn. J. Appl. Phys.*, vol. 41, pp. 6112–6118, 2002.

[23] C. J. Howard, T. M. Sabine, and F. Dickson, “Structural and thermal parameters for rutile and anatase,” *Acta Crystallogr. Sect. B*, vol. 47, no. 4, pp. 462–468, Aug. 1991.

[24] D. K. Pallotti, L. Passoni, P. Maddalena, F. Di Fonzo, and S. Lettieri, “Photoluminescence Mechanisms in Anatase and Rutile TiO 2 ".”

[25] J. R. Smyth, R. J. Swope, and A. R. Pawley, “H in rutile-type compounds: II. Crystal chemistry of Al substitution in H-bearing stishovite,” *American Mineralogist*, vol. 80, no. 5–6. pp. 454–456, Jun-1995.

[26] K. Mogyorósi, I. Dékány, and J. H. Fendler, “Preparation and characterization of clay mineral intercalated titanium dioxide nanoparticles,” *Langmuir*, vol. 19, no. 7, pp. 2938–2946, 2003.

[27] A. Ishii, Y. Nakamura, I. Oikawa, A. Kamegawa, and H. Takamura, “Low-temperature preparation of high-n TiO2 thin film on glass by pulsed laser deposition,” *Appl. Surf. Sci.*, vol. 347, pp. 528–834, 2015.

[28] S. Tang, J. Wang, Q. Zhu, Y. Chen, and X. Li, “Preparation of rutile TiO2 coating by thermal chemical vapor deposition for anticoking applications,” *ACS Appl. Mater. Interfaces*, vol. 6, no. 19, pp. 17157–17165, 2014.

[29] A. Ishii *et al.*, “Low-temperature preparation of rutile-type TiO2 thin films for optical coatings by aluminum doping,” *Appl. Surf. Sci.*, vol. 412, pp. 223–229, Aug. 2017.

[30] Y. K. Masakazu Anpo, Norikazu AIkawa, “Photoluminescence and Photocatalytic Activity of Highly Dispersed Titanium Oxide Anchored onto Porous Vycor Glass,” *J. Phys. Chem.*, vol. 89, no. 23, pp. 5017–5021, 1985.

[31] M. Anpo, T. Shima, and Y. Kubokawa, “ESR and Photoluminescence evidence for the photocatalytic formation of Hydroxyl radicals on small TiO2 particles", *Chem. Lett.*, vol. 14, no. 12, pp. 1799–1802, 1985.

[32] H. Tang, H. Berger, P. E. Schmid, F. Lévy, and G. Burri, “Photoluminescence in TiO2 anatase single crystals,” *Solid State Commun.*, vol. 87, no. 9, pp. 847–850, Sep. 1993.

[33] H. Tang, H. Berger, P. E. Schmid, and F. Lévy, “Optical properties of anatase (TiO2),” *Solid State Commun.*, vol. 92, no. 3, pp. 267–271, 1994.

[34] H. Tang, K. Prasad, R. Sanjinès, P. E. Schmid, and F. Lévy, “Electrical and optical properties of TiO2 anatase thin films,” *J. Appl. Phys.*, vol. 75, no. 4, pp. 2042–2047, 1994.

[35] W. F. Zhang, M. S. Zhang, and Z. Yin, “Microstructures and Visible Photoluminescence of TiO2 Nanocrystals,” *Phys. Status Solidi A*, vol. 179, no. 319, pp. 319–327, 2000.

[36] S. Mochizuki, T. Shimizu, and F. Fujishiro, “Photoluminescence study on defects in pristine anatase and anatase-based composites,” in *Physica B: Condensed Matter*, 2003, vol. 340–342, no. Supplement C, pp. 956–959.

[37] I. Fernández, A. Cremades, and J. Piqueras, “Cathodoluminescence study of defects in deformed (110) and (100) surfaces of TiO2 single crystals,” *Semicond. Sci. Technol.*, vol. 20, no. 2, pp. 239–243, 2005.

[38] R. Plugaru, A. Cremades, and J. Piqueras, “The effect of annealing in different atmospheres on the luminescence of polycrystalline TiO 2,” *J. Phys. Condens. Matter*, vol. 16, no. 2, pp. S261–S268, 2004.

[39] A. K. Ghosh, F. G. Wakim, and R. R. Addiss, “Photoelectronic processes in rutile,” *Phys. Rev.*, vol. 184, no. 3, pp. 979–988, 1969.

[40] Y. Nakato, H. Akanuma, Y. Magari, S. Yae, J. I. Shimizu, and H. Mori, “Photoluminescence from a bulk defect near the surface of an n-TiO2 (rutile) electrode in relation to an intermediate of photooxidation reaction of water,” *J. Phys. Chem. B*, vol. 101, no. 25, pp. 4934–4939, 1997.

BLOCK COPOLYMER TEMPLATED TIO_2 NANODOTS USING SOLUTION METHOD

Abstract

Block copolymer (BCP) lithography has received extensive attraction for the inorganic and metallic nanopatterning because of its self-assembled behavior, which offers different morphology of nanostructures. The BCP lithography method which is a combination of self-assembled BCP nanostructures fabrication and inorganic material deposition requires a low temperature inorganic deposition process to avoid polymer degradation. There are only few methods to synthesize the metal oxide and metals at low temperature. But in this paper, we are reporting solution method combining BCP template to synthesize TiO_2 nanostructures. A comparative study in between selective solution method and mask method will be presented. This BCP templated TiO_2 nanodots maintain the morphology of the template; which is a promising result for using this method to explore other self-assembled morphologies. Energy dispersive x-ray spectroscopy (EDX) confirms the presence of Ti and O_2 in the nanodot films, and x-ray diffraction (XRD) data shows mixture of both anatase and rutile TiO_2 crystalline phase. The photoluminescence (PL) spectrum for the synthesize TiO_2 is dominated by a broad peak extending from visible to near infrared (NIR), which consists of characteristic peaks for TiO_2 anatase (visible) and rutile phase (NIR). The fabricated closely-packed well-ordered TiO_2 nanodot films will be attractive for different optoelectronics, sensing and catalysis applications.

Introduction

Uniform periodic nanoscopic structures are getting significant attention because of their unique optical, electrical, magnetic and chemical properties in advanced technological field [1]. The properties of such a structure is determined by their shape, size, arrangements and materials. Several bottom up approaches such as various vapor deposition methods (e.g. atomic layer deposition (ALD), pulsed laser deposition (PLD) & chemical vapor deposition (CVD)), and chemical solution process etc. have been used for the synthesis of structures at the atomic or molecular level [2-5]. However, these methods are not yet self-sufficient enough for reproducibility, uniformity and large area patterns for devices. For the direct synthesis of nanostructure such a self-assembled materials-block copolymer (BCP) has received significant attention in different field of microelectronics and optoelectronic industry with low dimension and well-ordered patterning technology [6,7]. Different morphologies like lamellar, cylindrical and spherical which makes it suitable candidates for two and three dimensional lithographic processes [7-9]. Inorganic materials deposition in these BCP nanostructures leads to the formation of similar morphology of inorganic nanostructures. The shape and size of inorganic nanostructure can be tuned by varying the parameters like molecular ratio and volume fraction of BCP during synthesis [6,10].

The materials-with large band gap, high refractive index, high dielectric constant and high surface-activity is highly promising for semiconducting devices [11]. Titanium dioxide (TiO_2) is a highly promising semiconductor material with such unique structural and functional properties and very attractive in the area like photo catalysis, water splitting, solar cells, super capacitors and lithium-ion batteries [12–14]. Uniform ordered

TiO_2 nanostructure is even more attractive because of its improved optical and electrical properties such as high surface to volume ratio and conductivity compared to bulk [13-16]. So, a highly ordered, and superior quality TiO_2 materials are important criteria for the future optoelectronics and energy industry to thrive.

Herein, we are presenting an approach to fabricate well-ordered TiO_2 nanodots using BCP cylindrical nanostructures as templates. Solution method with two different condition at room temperature has been used as inorganic deposition method to fabricate the TiO_2 nanodots. In selective deposition method, the TiO2 materials follow the pattern of PMMA cylindrical structures while in mask method it just deposited in the void space of PMMA after PMMA is etched out. Field emission scanning electron microscopy (FESEM) and Atomic force microscopy (AFM) were used for microscopic imaging of the nanostructures, Energy dispersive x-ray spectroscopy (EDX) and x-ray diffraction (XRD) data were used to evaluate the TiO_2 nanodots structural property, and photoluminescence (PL) spectroscopy was done for investigating the optical property of these nanodots.

Experiments

BCP nanostructures fabrication. The substrates-Si wafer with thin layer of native oxide were cleaned by using mixture of hydrogen peroxide (H_2O_2), ammonium hydroxide (NH_4OH) and DI water (H_2O) at 65^oC for 2.5 hrs. A brush layer was deposited on the cleaned Si substrate to achieve perpendicular orientation of the BCP domains. The surface energy of the substrate plays vital role for the orientation of domain with substrate [17]. Polystyrene-random-polymethylmethacrylate (PS-r-PMMA) with

total molecular weight 156000 and 55 mole% PS with 1 wt.% toluene solution was deposited using spin casting method on cleaned Si-substrate as a brush layer. To graft properly the brush layer on the substrate surface, the layer was annealed at 240ºC on a hot plate inside a nitrogen atmosphere glove box for 40 minutes and then rinsed three times using toluene to remove the unreacted layer from the substrate. The BCP used in this study was polystyrene-block-polymethylmethacrylate (PS-b-PMMA) of molecular weight M_w 52000 (PS) and 142000 (PMMA); named here as PS52. The BCP layer was deposited on the brush layer grafted substrate from 1 wt% toluene solution using a spin coater. The samples, were then annealed in a muffle furnace (MTI Corporation KSL1100X) situated inside the glove box at 180 ºC for 24 hrs to facilitate microphase separation of PS and PMMA domains; which formed PS cylinders in PMMA matrix for this polymer with the above mentioned experimental conditions. All the chemicals were purchased from Sigma Aldrich and the polymers were purchased from Polymer Source Inc.

TiO_2 nanostructures deposition. In selective deposition method titanium (IV) bis (ammonium lactate) dihydroxide (TALH) from Sigma Aldrich was used as a titanium precursor to fabricate TiO_2 nanodots. A solution of titanium precursors TALH was made in such a way that aqueous solution of 0.20M TALH adjusted to pH 2.0 via addition of 1.0 M HCl. The sample with PS templates was immersed in to the solutions for different time interval: 12-18 hrs at room temperature. TALH was expected to interact only with PMMA which has active functional groups. The oxygen plasma with power 50Watt, flow rate 5.68Sccm and pressure 400mTorr for 60 Sec was used to remove the PS from the

sample. The samples were annealed into a furnace (MTI Corporation MTI 11000 X) at 500ºC for 7hrs in air; to remove any remaining polymers and to transform the amorphous TiO2 into crystal.

In the masked method, first PMMA domain was etched out selectively from the BCP nanostructured film. It is already well established that PMMA preferably etched compared to PS polymer during oxygen (O_2) plasma etching[18]. Here, controlled O_2 plasma etching with power 50W, flow rate 5.68 Sccm and 400mTorr pressure for 5 Sec was used to etch the PMMA domain selectively. The TiO2 was deposited using same recipe and same procedure as the selective deposition method experiments decribed above. TiO_2 was expected to deposit as a thin layer in the etched PMMA domain, as well on the PS cylinder surface.

Characterizations

Field emission scanning electron microscope (FESEM-Quanta 200) was used for the imaging of BCP and TiO_2 nanostructures samples. The elemental analysis of the TiO_2 nanostructures samples were done with the help of SEM energy dispersive x-ray spectroscopy (EDX) by using a field emission gun (Oxford Instruments) attached to the FESEM system. Surface morphology of the nanodot films were investigated using an atomic force microscope (Bruker-Dimension Icon). The AFM was done using 8 nm TESP Si tip in tapping mode. The AFM data were processed using Bruker NanoScope Analysis Suite 1.30 software. x-ray diffraction (XRD) measurements were done using a Bruker D8 Discover instrument operating at 40 kV and 40 mA. The XRD instrument with a characteristic x-ray source of Cu tube (Cu Kα, λ= 1.54184 Å) was used. The PL

measurements were done with a Horiba Labram HR Raman-PL system using 325 nm He-Cd laser.

Results and Discussion

The SEM image of the as grown microphase separated PS52 without any further treatment for imaging is shown in fig 20(a). A brush layer of PS-r-PMMA was used to promote the growth of vertical cylinder formation [17]. Following the BCP film casting on brush layered substrate annealing was done to promote the microphase separation of the domains; which leads a periodic arrangement of vertical cylindrical nanostructures. The diameter of cylinder and the domain size/cylinder to cylinder distance are presented in figure 20(b) and (c) as histogram plots. From the Gaussian curve fitting (figure 20(b) & (c) red curves) that, the average diameter of the cylinders is ~58 nm, and the average domain size of the cylinders are ~80 nm.

We were using the BCP cylindrical nanostructures as a template for TiO_2 nanostructure fabrication. In masked method, O_2 plasma etching was performed on the as grown BCP samples to etch PMMA domain and result a thin porous PS as mask. While in selective deposition method, BCP templates without etching was used. The different stages of fabrication are shown in Figure 21. Figure 21(a) and (b) show the SEM images of as grown PS-b-PMMA nanocylinder sample and the same sample after PMMA etching, respectively. The samples with PS templates (masked-method) and with PS-b-PMMA templates (selective deposition) were dipped in Titanium precursor solution at room temperature; which leads to formation of amorphous TiO_2 thin layer. In masked method, the TiO_2 deposited at the hole of porous PS templates while in selective

deposition method, the titania solution selectively interact with the PMMA templates of the PS-b-PMMA template samples. The PMMA molecule gas active functional groups carbonyl (C=O) and esters (C-O-H), which helps in the interactions with titania precursor, whereas PS is a hydrocarbon based polymer without any active functional group. For both methods, oxygen plasma etching was done to etch out the polymer and then annealed for 7 hrs at 500°C in air for the formation of crystalline TiO_2. Figure 21 shows the different stages of fabrication of TiO_2 nanodots. Figure 21(c) shows the SEM image of the same sample used in figure 21(a) & (b) after TiO2 deposition and polymer etching for mask method and figure 21(d) shows the SEM image of same sample used in Figure 21(a) & 21(b) after TiO2 deposition and polymer etching for selective deposition method.

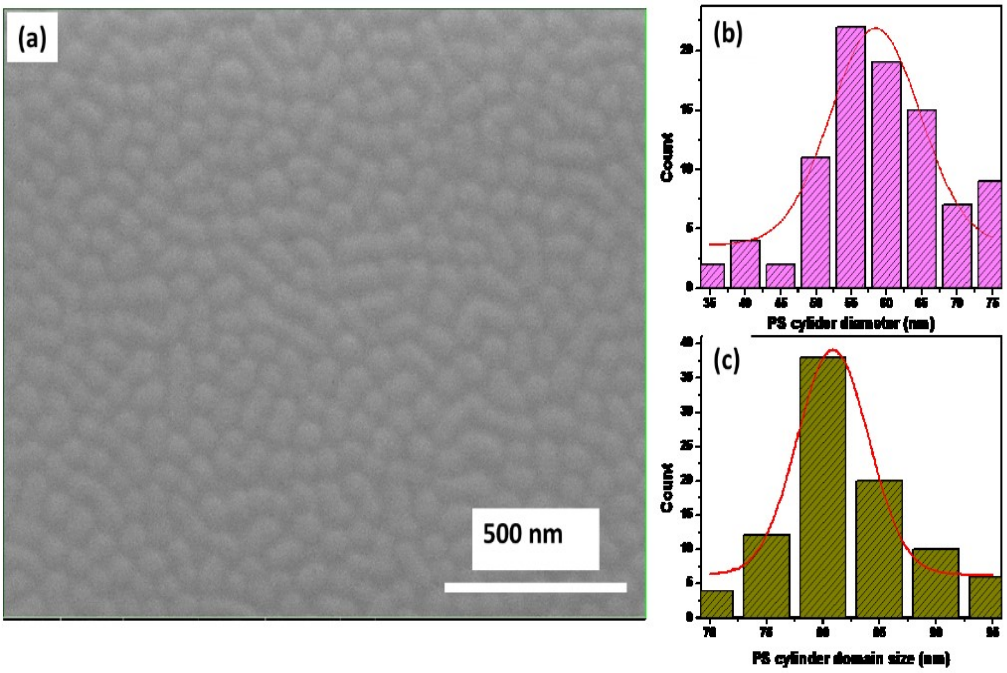

Figure 20. a) SEM image of as grown PS-b-PMMA BCP (PS52). Histogram plots for PS cylinder (a) diameter (average ~58nm) and (b) domain distance (average ~80nm)

Figure 22 shows the SEM and AFM images of the TiO_2 nanodots only sample and corresponding nanodot size and domain calculation from these images for mask method deposited sample. The structural properties of the masked deposited sample only are discussed here as it was difficult to characterize the selective deposition TiO_2 sample due to less deposition of TiO_2 materials by that method. Figure 22(c) & (e) show the histogram plots for the nanodot diameter and domain size, respectively derived from the SEM image 22(a). From the Gaussian fitting of the plot (figure 22 (c) & (e) red curves) the average diameter and domain size of TiO_2 nanodots only after annealing was noted as ~80 nm and ~40 nm, respectively. .Figure 22 (b) is the AFM topographical image of the same sample and figure 22(d) is the 3D projection of image 22(b). The average height of the nanodots are ~8 nm, calculated from depth histogram of the topographical image (figure 22(d)) using Bruker NanoScope Analysis Suite 1.30 (plot not shown). The average diameter of the nanodots calculated from the depth histogram of the AFM image is ~41 nm which is close to the average diameter calculated from the SEM image.
EDX spectroscopy attached to the SEM system was used to do elemental analysis of TiO_2 only nanodots to investigate and confirm the TiO_2 deposition. From EDX study, the presence of Ti and O was confirmed as shown in figure 23. The EDX spectrum is analyzed by the INCA software that runs the EDX detector and determines the atomic percentage of the elements present in the scanned area. The EDX spectrum recorded from the point of interest of TiO2 nanodots deposited by mask method (indicated as spectrum 1) shown in figure 23. The x-ray emission peaks at 0.452 (Ti L line), and 0.525 (O Kα line) are shown in the spectrum using corresponding Ti and O balloons. The most intense x-ray emission ~1.74 KeV (Si Kα line) is from the substrate, and the peak is not shown

here to focus the Ti and O peaks in the spectrum.

XRD was done to investigate the structural development of the TiO_2 nanodot only

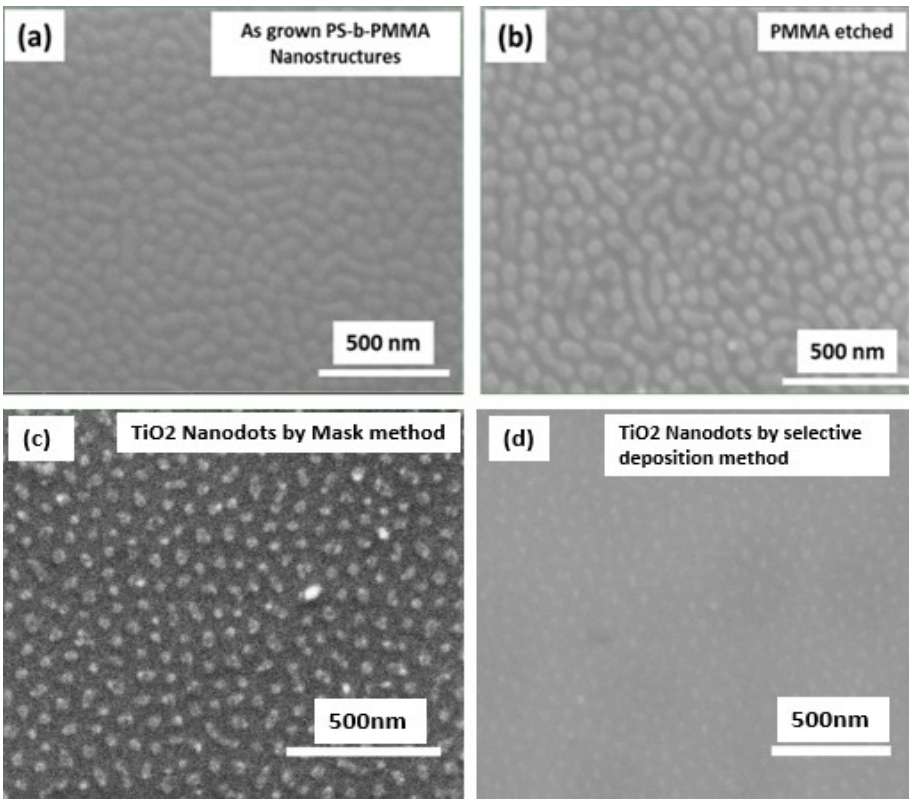

Figure 21. SEM images at different stage of fabrication of TiO2 Nanodots a) as-grown PS-b-PMMA nanostructures after phase separation, (b) PS cylinders after selective PMMA etching from the casted BCP nanostructured film, and (c) TiO2 only nanodots after removing polymer by oxygen plasma etching.

sample after annealing the material. Figure 24 shows the XRD 2θ plot for the TiO_2 nanodot sample; measurements were done using $CuK_{\alpha 5}$ radiation on x-ray diffractometer. The intensity of TiO_2 peak were very low in comparison to the peak coming from Si substrate. To eliminate the Si peak, the sample was tilted 7.8^o using chi rotation. The Bragg's diffraction peaks observed at 38. 67^o is corresponds to TiO_2 anatase (112) *hkl* plane and 44.97^o correspond to TiO_2 rutile phase with *hkl* plane of (210) respectively

[19–21]. The peak at Bragg's angle It is noted from the XRD data that, the rutile phase of TiO2 was observed at relatively low annealing temperature of 500oC compared to the usual high temperature for stable rutile phase formation [22,23].

In our case, TiO2 nanodots fabricated by selective deposition method, we could not have observed any corresponding EDX and XRD spectrum. This could be because of less amount of TiO2 deposition on the samples. Increasing the concentration of titanium precursor solution or tuning the time of deposition could be the way to increase the amount of TiO2 deposition.

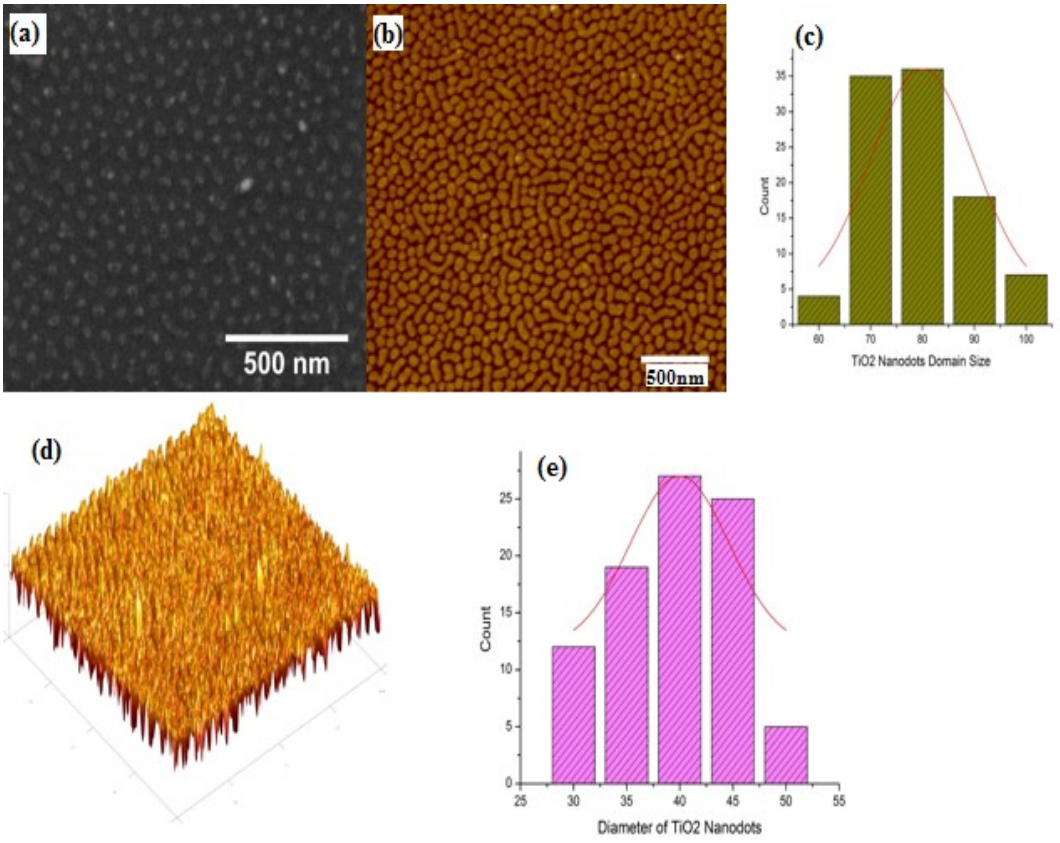

Figure 22. a) SEM image of TiO_2 nanodots by masked method after polymer etching. (c) and (e) are the histogram plots for the diameter and interdomain distance of the nanodots calculated from the SEM image shown in (a). (d) is the 3D projection of (b).

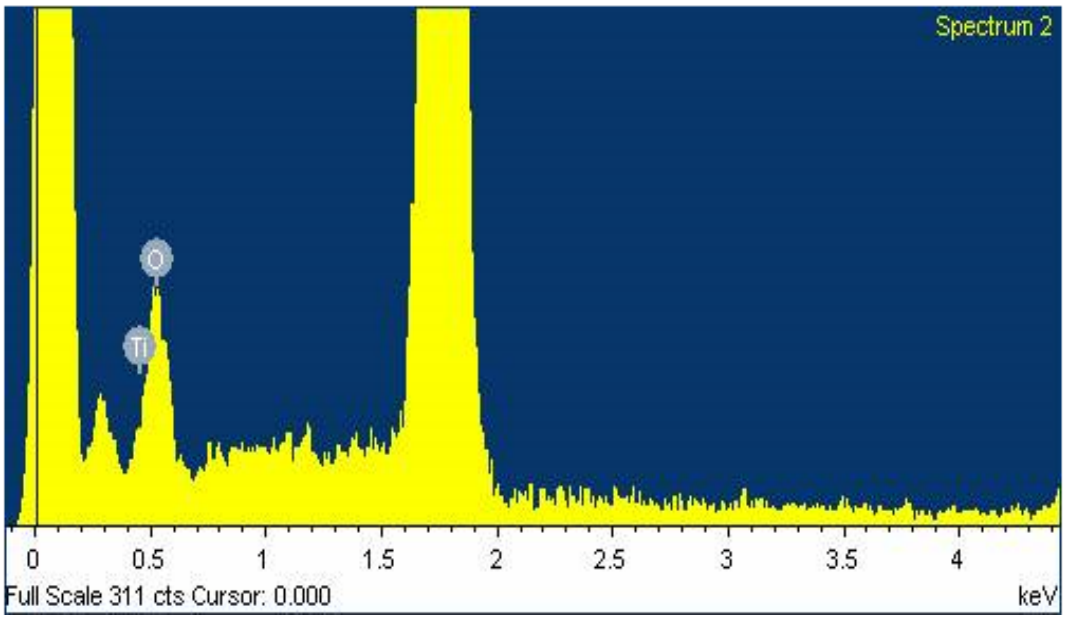

Figure 23. Elemental analysis of TiO_2 nanodots fabricated by masked method using EDX spectrum**.**

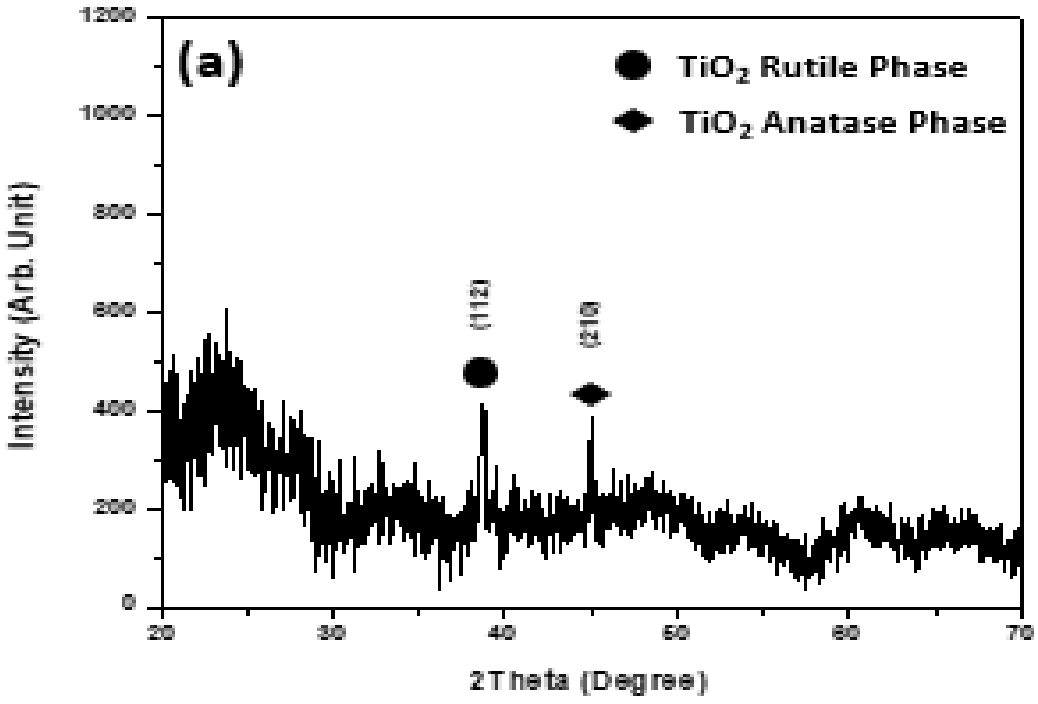

Figure 24. XRD 2θ plot of the TiO2 only nanodots fabricated by masked method as shown in the SEM and AFM image of figure 22.

Finally, the optical properties of these TiO_2 nanodots was performed on TiO_2 nanodots fabricated by both method using PL spectroscopy. The sample used for this study was the same sample shown in figure 21(c) and 21(d). The PL spectrum of the TiO_2 on both sample is dominated by a broad peak in the visible and near infrared (NIR) region (~1.5-2.6 eV) as shown in figure 25 (a) and (b) Which shows the characteristic peaks of TiO_2 anatase phase in the visible region and TiO_2 rutile phase in the NIR region [20,24–33]. The broad PL spectrum of anatase TiO_2 in the visible region is attributed to combination of different reasons such as self-trapped excitons, oxygen vacancies and defect sites, impurities or reduced metal ions, etc. [26–31]. The PL spectrum of rutile phase at NIR region broad peak is because of interstitial Ti^{3+} ions, trapped holes and free holes etc.[20,31–34] . Moreover, this PL spectrum also exhibits that the TiO_2 nanodots attributes with two TiO_2 crystalline phases; which agrees with the XRD data. But the PL intensity of mask deposited TiO_2 nanodots is more than the selective deposition. Which shows the mask deposition method is more effective in comparison to the selective deposition method

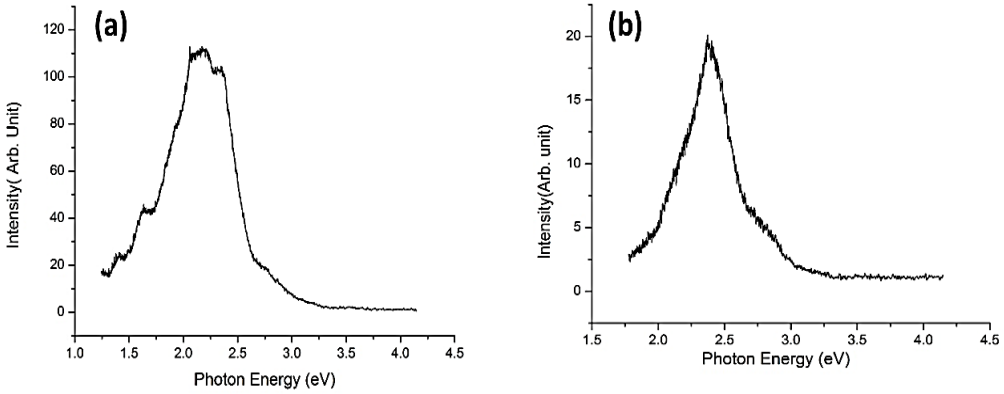

Figure 25. Room temperature PL spectrum of TiO2 nanodot sample showing a broad peak in the visible and NIR region (~1.5-2.6 eV) of the spectrum (a) for Mask method deposited TiO2 nanodots (b) for selective deposition method deposited TiO2 nanodots.

Conclusion

In summary, we successfully fabricated TiO_2 nanodots using BCP as template and solution method. High temperature annealing of the samples after deposition facilities crystallinity of the amorphous TiO_2 material, it also helped in the formation of these nanostructures from its thin film form. The deposited TiO_2 nanoparticles nucleated in the void PMMA domain space in between PS cylinders during high temperature (500 ^oC) annealing. The EDX elemental analysis confirms the presence of Ti and O atoms. The XRD and PL data shown the presence of mixed phase crystalline TiO_2 material. The broad PL spectrum in the visible and NIR spectral region supports the evidence of the anatase and rutile phase as shown by XRD.

References

[1] A. Ghicov and P. Schmuki, "Self-ordering electrochemistry: a review on growth and functionality of TiO2nanotubes and other self-aligned MOx structures," *Chem. Commun.*, no. 20, pp. 2791–2808, 2009.

[2] Z. Fan and J. G. Lu, "Zinc Oxide Nanostructures: Synthesis and Properties," *J. Nanosci. Nanotechnol.*, vol. 5, no. 10, pp. 1561–1573, 2005.

[3] M. Knez, K. Nielsch, and L. Niinistö, "Synthesis and Surface Engineering of Complex Nanostructures by Atomic Layer Deposition," *Adv. Mater.*, vol. 19, no. 21, pp. 3425–3438, 2007.

[4] C. N. R. Rao, F. L. Deepak, G. Gundiah, and A. Govindaraj, "Inorganic nanowires," *Prog. Solid State Chem.*, vol. 31, no. 1, pp. 5–147, 2003.

[5] S. C. ; Z. H. Singh, "Nanomaterials and Nanopatterns Based on Laser Processing: A Brief Review on Current State of Art," *Sci. Adv. Mater.*, vol. 4, no. 3–4, pp. 368–390, 2012.

[6] C. Park, J. Yoon, and E. L. Thomas, "Enabling nanotechnology with self-assembled block copolymer patterns," *Polymer (Guildf).*, vol. 44, no. 22, pp. 6725–6760, 2003.

[7] Y. C. Tseng and S. B. Darling, "Block copolymer nanostructures for technology," *Polymers*, vol. 2, no. 4. pp. 470–489, 2010.

[8] D. Y. Ryu, “A Generalized Approach to the Modification of Solid Surfaces,” *Science (80-.).*, vol. 308, no. 5719, pp. 236–239, 2005.

[9] C. A. Ross, K. K. Berggren, J. Y. Cheng, Y. S. Jung, and J.-B. Chang, “Three-Dimensional Nanofabrication by Block Copolymer Self-Assembly,” *Adv. Mater.*, vol. 26, no. 25, pp. 4386–4396, 2014.

[10] A. Nunns, J. Gwyther, and I. Manners, “Inorganic block copolymer lithography,” *Polym. (United Kingdom)*, vol. 54, no. 4, pp. 1269–1284, 2013.

[11] G. K. Mor, O. K. Varghese, M. Paulose, K. Shankar, and C. A. Grimes, “A review on highly ordered, vertically oriented TiO2 nanotube arrays: Fabrication, material properties, and solar energy applications,” *Sol. Energy Mater. Sol. Cells*, vol. 90, no. 14, pp. 2011–2075, 2006.

[12] S. M. Gupta and M. Tripathi, “A review of TiO2 nanoparticles,” *Chinese Sci. Bull.*, vol. 56, no. 16, pp. 1639–1657, 2011.

[13] V. P. Gupta and N. M. Ravindra, “Optoelectronic properties of rutile (TiO2),” *J. Phys. Chem. Solids*, vol. 41, no. 6, pp. 591–594, 1980.

[14] J. Tian, Z. Zhao, A. Kumar, R. I. Boughton, and H. Liu, “Recent progress in design, synthesis and applications of one-dimensional TiO2 nanostructured surface heterostructures: a review,” *Chem. Soc. Rev.*, vol. 43, no. 20, pp. 6920–6937, 2014.

[15] B. L. Ellis, P. Knauth, and T. Djenizian, “Three-dimensional self-supported metal oxides for advanced energy storage,” *Advanced Materials*, vol. 26, no. 21. pp. 3368–3397, 2014.

[16] A. Fakharuddin *et al.*, “Vertical TiO2 Nanorods as a Medium for Stable and High-Efficiency Perovskite Solar Modules,” *ACS Nano*, vol. 9, no. 8, pp. 8420–8429, 2015.

[17] P. Mansky, Y. Liu, E. Huang, T. P. Russell, and C. Hawker, “Con tro lling Polymer-Surface Interactions with Random Copolymer Brushes,” *Science (80-.).*, vol. 25, no. 7, pp. 1458–1460, 1997.

[18] T. H. Koji Asakawa, “Nanopatterning with Microdomains of Block Copolymers using Reactive-Ion Etching Selectivity Nanopatterning with Microdomains of Block Copolymers using Reactive-Ion Etching Selectivity,” *Jpn. J. Appl. Phys.*, vol. 41, pp. 6112–6118, 2002.

[19] C. J. Howard, T. M. Sabine, and F. Dickson, “Structural and thermal parameters for rutile and anatase,” *Acta Crystallogr. Sect. B*, vol. 47, no. 4, pp. 462–468, Aug. 1991.

[20]D. K. Pallotti, L. Passoni, P. Maddalena, F. Di Fonzo, and S. Lettieri, “Photoluminescence Mechanisms in Anatase and Rutile TiO2,” *J. Phys. Chem. C*, vol. 121, no. 16, pp. 9011–9021, 2017.

[21] J. R. Smyth, R. J. Swope, and A. R. Pawley, “H in rutile-type compounds: II. Crystal chemistry of Al substitution in H-bearing stishovite,” *American Mineralogist*, vol. 80, no. 5–6. pp. 454–456, Jun-1995.

[22] S. Tang, J. Wang, Q. Zhu, Y. Chen, and X. Li, “Preparation of rutile TiO2 coating by thermal chemical vapor deposition for anticoking applications,” *ACS Appl. Mater. Interfaces*, vol. 6, no. 19, pp. 17157–17165, 2014.

[23] A. Ishii *et al.*, “Low-temperature preparation of rutile-type TiO2 thin films for optical coatings by aluminum doping,” *Appl. Surf. Sci.*, vol. 412, pp. 223–229, Aug. 2017.

[24] Y. K. Masakazu Anpo, Norikazu AIkawa, “Photoluminescence and Photocatalytic Activity of Highly Dispersed Titanium Oxide Anchored onto Porous Vycor Glass,” *J. Phys. Chem.*, vol. 89, no. 23, pp. 5017–5021, 1985.

[25] M. Anpo, T. Shima, and Y. Kubokawa, “ESR and Photoluminescence evidence for the photocatalytic formation of hydroxyl radicals on small TiO2 particles", *Chem. Lett.*, vol. 14, no. 12, pp. 1799–1802, 1985.

[26] H. Tang, H. Berger, P. E. Schmid, F. Lévy, and G. Burri, “Photoluminescence in TiO2 anatase single crystals,” *Solid State Commun.*, vol. 87, no. 9, pp. 847–850, Sep. 1993.

[27] H. Tang, H. Berger, P. E. Schmid, and F. Lévy, “Optical properties of anatase (TiO2),” *Solid State Commun.*, vol. 92, no. 3, pp. 267–271, 1994.

[28] H. Tang, K. Prasad, R. Sanjinès, P. E. Schmid, and F. Lévy, “Electrical and optical properties of TiO2 anatase thin films,” *J. Appl. Phys.*, vol. 75, no. 4, pp. 2042–2047, 1994.

[29] W. F. Zhang, M. S. Zhang, and Z. Yin, “Microstructures and Visible Photoluminescence of TiO2 Nanocrystals,” *Phys. Status Solidi A*, vol. 179, no. 319, pp. 319–327, 2000.

[30] S. Mochizuki, T. Shimizu, and F. Fujishiro, “Photoluminescence study on defects in pristine anatase and anatase-based composites,” in *Physica B: Condensed Matter*, 2003, vol. 340–342, no. Supplement C, pp. 956–959.

[31]I. Fernández, A. Cremades, and J. Piqueras, “Cathodoluminescence study of defects in deformed (110) and (100) surfaces of TiO2 single crystals,” *Semicond. Sci. Technol.*, vol. 20, no. 2, pp. 239–243, 2005.

[32] R. Plugaru, A. Cremades, and J. Piqueras, “The effect of annealing in different atmospheres on the luminescence of polycrystalline TiO 2,” *J. Phys. Condens. Matter*, vol. 16, no. 2, pp. S261–S268, 2004.

[33] A. K. Ghosh, F. G. Wakim, and R. R. Addiss, “Photoelectronic processes in rutile,” *Phys. Rev.*, vol. 184, no. 3, pp. 979–988, 1969.

[34] Y. Nakato, H. Akanuma, Y. Magari, S. Yae, J. I. Shimizu, and H. Mori, “Photoluminescence from a bulk defect near the surface of an n-TiO2 (rutile) electrode in relation to an intermediate of photooxidation reaction of water,” *J. Phys. Chem. B*, vol. 101, no. 25, pp. 4934–4939, 1997.

CONCLUSION

A study of BCP nanostructure morphological evolution along with fabrication of TiO_2 nanodots were performed. In first study, PMMA cylinder in PS matrix forming PS-b-PMMA BCP (PMMA22) was used to see the variation in BCP morphology and orientation by changing different parameters. It is shown that the perpendicular orientation of BCP domains largely depend on preferential wetting layer between substrate and BCP interface, the nature and solution concentration of brush polymer. It is also shown that the perpendicular orientation is observed when thickness of BCP thin film is within the range of domain size multiples. The annealing time and temperature studies shows that the time and temperature need to be optimized for obtaining perpendicular orientation.

In the second and third works, TiO_2 nanodots were successfully fabricated at room temperature using perpendicularly oriented BCP nanostructure as templates. Two novel approaches - PLD and Solution method were used separately to deposit the TiO_2 nanodots. The nanostructure analysis using SEM, PL, XRD and EDX justified the presence of TiO_2 on the sample. Presence of different TiO_2 *hkl* planes belongs to different Braggs diffraction angle shows the nucleation of both rutile and anatase phase of TiO_2. The broad PL peak in the visible and NIR spectral region provides extra supports to the information presented by XRD regarding TiO_2 dual phases. Large XRD and PL intensity for PLD deposited TiO_2 compared to solution deposited method show that PLD method is more effective in depositing better quality of material. Basically, this approach combining PLD method with BCP as templates open a new door to fabricate inorganic

nanostructures; moreover we have shown formation of rutile phase of TiO_2 at relatively low temperature.

REFERENCES

[1] Y. Xia, J. A. Rogers, K. E. Paul, and G. M. Whitesides, "Unconventional Methods for Fabricating and Patterning Nanostructures," *Chem. Rev.*, vol. 99, no. 7, pp. 1823–1848, 1999.

[1] Y. Xia, J. A. Rogers, K. E. Paul, and G. M. Whitesides, "Unconventional Methods for Fabricating and Patterning Nanostructures," *Chem. Rev.*, vol. 99, no. 7, pp. 1823–1848, 1999.

[2] C. Q. Sun, "Size dependence of nanostructures: Impact of bond order deficiency," *Progress in Solid State Chemistry*, vol. 35, no. 1. pp. 1–159, 2007.

[3] M. Ramanathan, S. M. Kilbey, II, Q. Ji, J. P. Hill, and K. Ariga, "Materials self-assembly and fabrication in confined spaces," *J. Mater. Chem.*, vol. 22, no. 21, p. 10389, 2012.

[4] A. del Campo and E. Arzt, "Fabrication approaches for generating complex micro- and nanopatterns on polymeric surfaces," *Chemical Reviews*, vol. 108, no. 3. pp. 911–945, 2008.

[5] Z. Fan and J. G. Lu, "Zinc Oxide Nanostructures: Synthesis and Properties," *J. Nanosci. Nanotechnol.*, vol. 5, no. 10, pp. 1561–1573, 2005.

[6] M. Knez, K. Nielsch, and L. Niinistö, "Synthesis and Surface Engineering of Complex Nanostructures by Atomic Layer Deposition," *Adv. Mater.*, vol. 19, no. 21, pp. 3425–3438, 2007.

[7] R. N. Hall, "Inorganic nanowires," *Phys. Rev.*, vol. 87, no. 2, pp. 387–387, 1952.

[8] S. C. ; Z. H. Singh, "Nanomaterials and Nanopatterns Based on Laser Processing: A Brief Review on Current State of Art," *Sci. Adv. Mater.*, vol. 4, no. 3–4, pp. 368–390, 2012.

[9] C. A. Mack, "The Future of Semiconductor Lithography : After Optical , What Next ?," *Online*, vol. 23, pp. 1–5, 2007.

[10] I. W. Hamley, "The Physics of Block Copolymers," 1998.

[11] R. D. Peters, X. M. Yang, T. K. Kim, and P. F. Nealey, "2000_Langmuir_Wetting Behavior of Block Copolymers on Self-Assembled Films of Alkylchlorosiloxanes_Effect of Grafting Density.pdf," *Langmuir*, vol. 16, no. 24, pp. 9620–9626, 2000.

[12] H.-C. Kim, S.-M. Park, and W. D. Hinsberg, "Block Copolymer Based Nanostructures: Materials, Processes, and Applications to Electronics," *Chem.*

Rev., vol. 110, no. 1, pp. 146–177, 2010.

[13] H. C. Kim *et al.*, "A route to nanoscopic SiO2 posts via block copolymer templates," *Adv. Mater.*, vol. 13, no. 11, pp. 795–797, 2001.

[14] R. Farrell, T. G. Fitzgerald, D. Borah, J. D. Holmes, and M. Morris, "Chemical interactions and their role in the microphase separation of block copolymer thin films.," *International journal of molecular sciences*, vol. 10, no. 9, pp. 3671–712, 2009.

[15] J. R. Fried, *Polymer Science and Technology*, Third. Prentice Hall, 2014.

[16] Gilman Ewan Stephen Toombes, "Structural Studies Of Block Copolymer And Block Copolymer/Aluminosilicate Materials," Cornell University.

[17] G. M. Whitesides, J. P. Mathias, and C. T. Seto, "Articles Molecular and A Chemical Strategy for the Synthesis of Nanostructures," *Science (80-.).*, vol. 254, no. 5036, pp. 1312–1319, 1991.

[18] F. Würthner, "Perylene bisimide dyes as versatile building blocks for functional supramolecular architectures," *Chem. Commun.*, no. 14, pp. 1564–1579, 2004.

[19] B. Olenyuk, J. A. Whiteford, A. Fechtenkötter, and P. J. Stang, "Self-assembly of nanoscale cuboctahedra by coordination chemistry," *Nature*, vol. 398, no. April, pp. 796–799, 1999.

[20] F. S. Bates and G. H. Fredrickson, "Block Copolymer Thermodynamics: Theory and Experiment," *Annu. Rev. Phys. Chem.*, vol. 41, no. 1, pp. 525–557, 1990.

[21] J. Melenkevitz and M. Muthukumar, "Density Functional Theory of Lamellar Ordering in Diblock Copolymers," *Macromolecules*, vol. 24, no. 14, pp. 4199–4205, 1991.

[22] P. D. Topham, A. J. Parnell, and R. C. Hiorns, "Block copolymer strategies for solar cell technology," *Journal of Polymer Science, Part B: Polymer Physics*, vol. 49, no. 16. pp. 1131–1156, 2011.

[23] Y. C. Tseng and S. B. Darling, "Block copolymer nanostructures for technology," *Polymers*, vol. 2, no. 4. pp. 470–489, 2010.

[24] J. M. G. Swann and P. D. Topham, "Design and application of nanoscale actuators using block-copolymers," *Polymers*, vol. 2, no. 4. pp. 454–469, 2010.

[25] C. Park, J. Yoon, and E. L. Thomas, "Enabling nanotechnology with self assembled block copolymer patterns," *Polymer (Guildf).*, vol. 44, no. 22, pp. 6725–6760, 2003.

[26] A. Andreozzi, E. Poliani, G. Seguini, and M. Perego, "The effect of random

copolymer on the characteristic dimensions of cylinder-forming PS- *b* -PMMA thin films," *Nanotechnology*, vol. 22, no. 18, p. 185304, 2011.

[27] I. A. Zucchi, E. Poliani, and M. Perego, "Microdomain orientation dependence on thickness in thin films of cylinder-forming PS- b -PMMA," *Nanotechnology*, vol. 21, no. 18, p. 185304, 2010.

[28] X. Gu, I. Gunkel, and T. P. Russell, "Pattern Transfer Using Block Copolymers," *Philos. Trans. R. Soc. A Math. Phys. Eng. Sci.*, vol. 371, no. 2000, pp. 20120306–20120306, 2013.

[29] S. H. Kim, M. J. Misner, T. Xu, M. Kimura, and T. P. Russell, "Highly Oriented and Ordered Arrays from Block Copolymers via Solvent Evaporation," *Adv. Mater.*, vol. 16, no. 3, pp. 226–231, 2004.

[30] T. Thurn-Albrecht, J. DeRouchey, T. P. Russell, and R. Kolb, "Pathways Toward Electric Field Induced Alignment Of Block Copolymers," *Macromolecules*, vol. 35, no. 21, pp. 8106–8110, 2002.

[31] X. Yu, J. Peng, L. Cui, H. Wang, B. Li, and Y. Han, "Morphology Development Of Ultrathin Symmetric Diblock Copolymer Film Via Solvent Vapor Treatment," *Macromolecules*, vol. 37, no. 19, pp. 7301–7307, 2004.

[32] T. Thurn-Albrecht, J. Derouchey, T. P. Russell, and H. M. Jaeger, "Overcoming Interfacial Interactions With Electric Fields," *Macromolecules*, vol. 33, no. 9, pp. 3250–3253, 2000.

[33] Ossila, "A Guide to Theory and Techniques Introduction to Spin Coating Special Requirements for Spin Coating Nanoparticles," no. 1. pp. 1–24, 2016.

[34] R. D. Peters, X. M. Yang, T. K. Kim, B. H. Sohn, and P. F. Nealey, "Using self-assembled monolayers exposed to X-rays to control the wetting behavior of thin films of diblock copolymers," *Langmuir*, vol. 16, no. 10, pp. 4625–4631, 2000.

[35] D. Borah, M. Ozmen, S. Rasappa, M. T. Shaw, J. D. Holmes, and M. A. Morris, "Molecularly functionalized silicon substrates for orientation control of the microphase separation of PS-b-PMMA and PS-b-PDMS block copolymer systems," *Langmuir*, vol. 29, no. 9, pp. 2809–2820, 2013.

[36] K. Sparnacci *et al.*, "Ultrathin Random Copolymer-Grafted Layers for Block Copolymer Self-Assembly," *ACS Appl. Mater. Interfaces*, vol. 7, no. 20, pp. 10944–10951, 2015.

[37] P. Mansky, Y. Liu, E. Huang, T. P. Russell, and C. Hawker, "Con tro lling Polymer-Surface Interactions with Random Copolymer Brushes," *Science (80-.).*, vol. 25, no. 7, pp. 1458–1460, 1997.

[38] D. Y. Ryu, "A Generalized Approach to the Modification of Solid Surfaces,"

Science (80-.)., vol. 308, no. 5719, pp. 236–239, 2005.

[39] S. P-smmaran, "Sample Name : Random Copolymer Poly (styrene-co-methyl methacrylate)."

[40] "Sample Name : ω - Hydroxy Terminated Polystyrene Sample #: P18848 SOH Structure : H 3 C n H SEC of Sample : Sample ID : P18848-SOH Composition : Synthesis Procedure : ω , -hydroxy terminated polystyrene was prepared by living anionic polymerization using," p. 18848.

[41] S. H. Anastasiadis, T. P. Russell, S. K. Satija, and C. F. Majkrzak, "Neutron reflectivity studies of the surface-induced ordering of diblock copolymer films," *Phys. Rev. Lett.*, vol. 62, no. 16, pp. 1852–1855, 1989.

[42] G. Coulon, T. P. Russell, V. R. Deline, and P. F. Green, "Surface-Induced Orientation of Symmetric, Diblock Copolymers: A Secondary Ion Mass Spectrometry Study," *Macromolecules*, vol. 22, no. 6, pp. 2581–2589, 1989.

[43] A. Menelle, T. P. Russell, S. H. Anastasiadis, S. K. Satija, and C. F. Majkrzak, "Ordering of thin diblock copolymer films," *Phys. Rev. Lett.*, vol. 68, no. 1, pp. 67–70, 1992.

[44] G. H. Fredrickson and E. Helfand, "Fluctuation effects in the theory of microphase separation in block copolymers," *J. Chem. Phys.*, vol. 87, no. 1, pp. 697–705, 1987.

[45] R. A. Segalman, "Patterning with block copolymer thin films," *Materials Science and Engineering R: Reports*, vol. 48, no. 6. pp. 191–226, 2005.

[46] L. V. and M. del R. R.-H. cesar soto-figueroa, "Thermal Study on Phase Transitions of Block Copolymers by Mesoscopic Simulation," *Adv. Chem. Eng.*

[47] D. U. Ahn and E. Sancakta, "Temperature-dependent phase behaviors in cylinder-forming block copolymers," *Int. J. Mol. Sci.*, vol. 10, no. 5, pp. 2169–2189, 2009.

[48] B. Lindman and P. Alexandridis, *Amphiphilic block copolymers : self-assembly and applications*. Amsterdam; New YOrk: Elsevier, 2000.

[49] L. Zhang and A. Eisenberg, "Multiple Morphologies of 'Crew-Cut' Aggregates of Polystyrene-b-poly(acrylic acid) Block Copolymers," *Science (80-.).*, vol. 268, no. 5218, pp. 1728–1731, 1995.

[50] F. H. Schacher, P. A. Rupar, and I. Manners, "Functional block copolymers: Nanostructured materials with emerging applications," *Angewandte Chemie - International Edition*, vol. 51, no. 32. pp. 7898–7921, 2012.

[51] M. Ulbricht, "Advanced functional polymer membranes," *Polymer (Guildf).*, vol. 47, no. 7, pp. 2217–2262, 2006.

[52] W. A. Phillip, B. O'neill, M. Rodwogin, M. A. Hillmyer, and E. L. Cussler, "Self-assembled block copolymer thin films as water filtration membranes," *ACS Appl. Mater. Interfaces*, vol. 2, no. 3, pp. 847–853, 2010.

[53] J. H. Moon and S. Yang, "Chemical aspects of three-dimensional photonic crystals," *Chem. Rev.*, vol. 110, no. 1, pp. 547–574, 2010.

[54] Y. Kang, J. J. Walish, T. Gorishnyy, and E. L. Thomas, "Broad-wavelength-range chemically tunable block-copolymer photonic gels," *Nat. Mater.*, vol. 6, no. 12, pp. 957–960, 2007.

[55] B. S. Förster and M. Antonietti, "Amphiphilic Block Copolymers in Structure-Controlled Nanomaterial Hybrids," *Adv. Mater.*, vol. 10, no. 3, pp. 195–217, 1998.

[56] M. S. Aw, K. Gulati, and D. Losic, "Controlling Drug Release from Titania Nanotube Arrays Using Polymer Nanocarriers and Biopolymer Coating," *J. Biomater. Nanobiotechnol.*, vol. 2, no. 5, pp. 477–484, 2011.

[57] C. Oerlemans, W. Bult, M. Bos, G. Storm, J. F. W. Nijsen, and W. E. Hennink, "Polymeric micelles in anticancer therapy: Targeting, imaging and triggered release," *Pharm. Res.*, vol. 27, no. 12, pp. 2569–2589, 2010.

[58] J. L. Tan, J. Tien, D. M. Pirone, D. S. Gray, K. Bhadriraju, and C. S. Chen, "Cells lying on a bed of microneedles: An approach to isolate mechanical force," *Proc. Natl. Acad. Sci.*, vol. 100, no. 4, pp. 1484–1489, 2003.

[59] P. Khanna, J. A. Strom, J. I. Malone, and S. Bhansali, "Microneedle-Based Automated Therapy for Diabetes Mellitus," *J. Diabetes Sci. Technol.*, vol. 2, no. 6, pp. 1122–1129, 2008.